



Surface characterization of pan-ba  
by K Battleson

A thesis submitted in partial fulfillment of the requirements for the degree of Master of Science in  
Chemical Engineering  
Montana State University  
© Copyright by K Battleson (1998)

Abstract:

Carbon-epoxy materials are finding increased structural uses in areas such as aerospace, aeronautical, and sporting goods applications because they can be produced with desirable strength-to-weight properties. Historically, the limiting factor to the strength of those composites has been the integrity of the fiber-resin interface bond. Recently, surface analysis methods have been introduced to study this fiber/matrix interface.

In this study, SIMS, XPS, and AFM were used to characterize both untreated and electrochemically treated PAN-based carbon fibers. Hexcel Corp. provided the fibers studied and included poor quality fibers from lots with mechanical properties that failed to meet the product specification as well as fibers from good quality lots. It was hypothesized that the poor mechanical performance observed in some of the fiber lots was the result of either chemical or topographic abnormalities in the fibers. It was proposed that these abnormalities could be detected by the surface sensitive techniques mentioned.

Multivariate statistical techniques were used to explore relationships between the SIMS spectra and the mechanical test results. Principal components analysis (PCA) and discriminant analysis with cross validation were used to analyze the SIMS spectra of both treated and untreated fibers. Statistically significant differences in the surface chemistry of "good" and "poor" quality fibers were identified in both treated and untreated fibers. The PCA and discriminant loadings assisted in identifying the chemistry of changes in both inorganic and organic functionalities on the poor quality fibers. These changes include an increase of oxygen on poor property untreated fiber spectra, an increase of unsaturated hydrocarbon fragments on good property untreated fiber spectra, and differences in the amount of aluminum, PDMS, magnesium, calcium, and potassium. Treated fibers primarily differed in magnesium and calcium concentrations, as well. The resulting analysis also includes that there was an increase in nitrogen containing fragments on the spectra of poor property fibers.

Preliminary Atomic Force Microscopy analysis found differences in topography correlating to the mechanical properties; however, more work would be needed to determine whether variations are statistically significant.

SURFACE CHARACTERIZATION OF PAN-BASED CARBON FIBERS

USING XPS, SIMS, AND AFM

by

Kris Anne Battleson

A thesis submitted in partial fulfillment  
of the requirements for the degree

of

Master of Science

in

Chemical Engineering

MONTANA STATE UNIVERSITY-BOZEMAN  
Bozeman, Montana

August, 1998

N378  
B3199

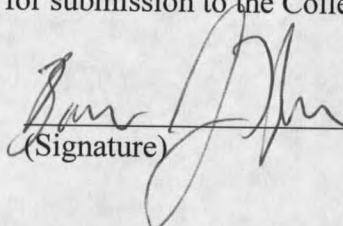
APPROVAL

of a thesis submitted by

Kris Anne Battleson

This thesis has been read by each member of the thesis committee and has been found to be satisfactory regarding content, English usage, format, citations, bibliographic style, and consistency, and is ready for submission to the College of Graduate Studies.

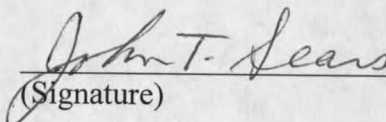
Dr. Bonnie J. Tyler

  
(Signature)

8/27/98  
Date

Approved for the Department of Chemical Engineering

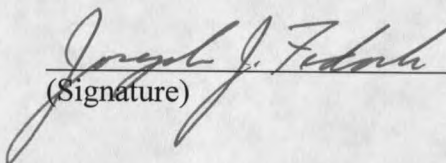
Dr. John T. Sears

  
(Signature)

8/27/98  
Date

Approved for the College of Graduate Studies

Dr. Joseph J. Fedock

  
(Signature)

8/28/98  
Date

## STATEMENT OF PERMISSION TO USE

In presenting this thesis in partial fulfillment of the requirements for a master's degree at Montana State University-Bozeman, I agree that the Library shall make it available to borrowers under rules of the Library.

If I have indicated my intention to copyright this thesis by including a copyright notice page, copying is allowable only for scholarly purposes, consistent with "fair use" as prescribed in the U.S. Copyright Law. Requests for permission for extended quotation from or reproduction of this thesis in whole or in parts may be granted only by the copyright holder.

Signature Kus Bat

Date 8/27/98

## ACKNOWLEDGEMENTS

The author wishes to thank Dr. Bonnie Tyler and Dr. Doug Cairns for their guidance throughout this project and the Imaging and Chemical Analysis Laboratory at Montana State University for help with all instrumentation. Thanks are also given to Dr. John Sears for serving as a graduate committee member and Dan Samborsky for all of his computer expertise. Finally thanks to Hexcel and NSF for funding this project.

## TABLE OF CONTENTS

	Page
LIST OF TABLES .....	vii
LIST OF FIGURES .....	viii
ABSTRACT .....	xii
<b>1. INTRODUCTION.....</b>	<b>1</b>
Problem in This Area .....	1
Motivation for Research .....	2
Research Objectives.....	3
<b>2. BACKGROUND .....</b>	<b>4</b>
Analytical Methods.....	4
X-ray Photoelectron Spectroscopy.....	4
Theory and Principles of the Technique .....	4
Previous Work on Carbon Fiber Surfaces .....	10
Secondary Ion Mass Spectrometry .....	14
Theory and Principles of the Technique .....	14
Previous Work on Carbon Fiber Surfaces .....	17
Atomic Force Microscopy .....	18
Theory and Principles of the Technique .....	19
Previous Work on Carbon Fiber Surfaces .....	21
Numerical Methods.....	21
Principal Components Analysis.....	21
Theory and Principles of the Technique .....	22
Previous Work on Carbon Fiber Surfaces .....	25
Discriminant Function Analysis .....	26
Theory and Principles of the Technique .....	26
Cross Validation.....	27
Theory and Principles of the Technique .....	27
<b>3. EXPERIMENTAL METHODS AND MATERIALS .....</b>	<b>28</b>
Analytical Methods.....	28
SIMS Analysis .....	28
XPS Analysis .....	31
AFM Analysis .....	32
Numerical Methods.....	32
<b>4. RESULTS.....</b>	<b>33</b>
Untreated Fiber Spools .....	33

**TABLE OF CONTENTS- Continued**

	Page
Secondary Ion Mass Spectrometry .....	34
Atomic Force Microscopy .....	42
Treated Fiber Spools .....	48
Secondary Ion Mass Spectrometry .....	48
X-ray Photoelectron Spectroscopy.....	58
Atomic Force Microscopy .....	60
Variable Treated Fibers.....	65
Secondary Ion Mass Spectrometry .....	65
X-ray Photoelectron Spectroscopy.....	69
5. CONCLUSION.....	72
Untreated Fibers.....	72
Treated Fibers .....	72
Variable Treated Fibers.....	73
Future Work and Recommendations .....	73
REFERENCES CITED.....	75
APPENDICES.....	78
Appendix A- Fiber Sample Identification.....	79
Appendix B- Fiber Sample SIMS Spectra.....	86
Appendix C- Complete Peak Area Matrices.....	153
Appendix D- MATLAB™ Programs.....	232
Appendix E- Fragmentation Pieces Listed by Atomic Mass.....	236

**LIST OF TABLES**

Table	Page
1. Information obtained by x-ray photoelectron spectroscopy from Ratner and Castner .....	5
2. Common binding energy assignments for the carbon 1s peak from Ratner and Castner .....	9
3. Common binding energy assignments for the oxygen 1s peak from Ratner and Castner .....	9
4. Advantages and disadvantages of contact mode AFM from <i>Digital Instruments Scanning Probe Microscopy Training Notebook</i> .....	20
5. Advantages of principal components analysis from Malinowski .....	22
6. Fiber lot mechanical property descriptions.....	29
7. Atomic concentrations for D1374-6A and D1424-6C .....	60
8. Atomic concentrations for D1239-3C variable treated fibers .....	71
9. Calculated F values and confidence levels .....	71

## LIST OF FIGURES

Figure	Page
1. Schematic of x-ray photoelectron spectroscopy .....	7
2. Schematic of a carbon atom undergoing the photoelectron process .....	8
3. High resolution carbon 1s peak of untreated carbon fiber by Sherwood et al.....	12
4. High resolution carbon 1s peak of surface treated carbon fiber by Sherwood et al. ....	13
5. Schematic of secondary ion mass spectrometry .....	15
6. Schematic showing the components of contact mode atomic force microscopy.....	19
7. Graphical representation of principal components analysis .....	24
8. An illustration of the discriminant function for a two-dimensional case .....	26
9. Loading #1 shows a variance in aluminum concentration ( $m/z = 27$ ) in the untreated fiber group .....	35
10. Loading #2 shows a variance in PDMS concentration ( $m/z = 28, 73, 147$ ) in the untreated fiber group.....	35
11. Loading #3 shows a variance in magnesium concentration ( $m/z = 24$ ), potassium concentration ( $m/z = 39$ ), calcium concentration ( $m/z = 40$ ), and PDMS concentration ( $m/z = 28, 73, 147$ ) in the untreated fiber group .....	36
12. Discriminant analysis with cross validation correctly identified differences between good and poor property untreated fibers.....	37
13. Discriminant loadings show the differences in good and poor untreated fibers can be attributed to organic components .....	38
14. Loading #1 shows a variance in PDMS concentration ( $m/z = 73, 147$ ) in the untreated fiber group.....	39

15. Discriminant analysis with cross validation correctly identified differences between good and poor property untreated fibers using organic components .....	40
16. Discriminant loadings show the differences in good and poor untreated fibers .....	40
17. Discriminant analysis with cross validation correctly identified differences between good and poor property untreated fibers using organic components in the absence of PDMS .....	41
18. Discriminant loadings show organic differences between good and poor property untreated fibers can be attributed to organic components other than PDMS .....	42
19. Surface contour plot of R128-04 (good property) fiber .....	44
20. Surface contour plot of R128-08 (poor property) fiber .....	44
21. Horizontal section plot of R128-04 (good property) fiber .....	45
22. Horizontal section plot of R128-08 (poor property) fiber .....	45
23. Vertical section plot of R128-04 (good property) fiber .....	46
24. Vertical section plot of R128-08 (poor property) fiber.....	46
25. Scanning electron microscope image of R128-04 (good property) fiber .....	47
26. Scanning electron microscope image of R128-08 (poor property) fiber .....	47
27. Loading #1 shows a variance in magnesium concentration ( $m/z = 24$ ) and calcium concentration ( $m/z = 40$ ) in the treated fiber group .....	49
28. Loading #2 shows a variance in aluminum concentration ( $m/z = 27$ ) in the treated fiber group .....	49
29. Loading #3 shows a variance in PDMS concentration ( $m/z = 28, 73, 147$ ) in the treated fiber group.....	50
30. Loading #4 shows a variance in PDMS concentration ( $m/z = 28, 73, 147$ ) and potassium concentration ( $m/z = 39$ ) in the treated fiber group .....	50

31. Loading #5 shows a variance in potassium concentration ( $m/z = 39$ ), chromium concentration ( $m/z = 52$ ), and iron concentration ( $m/z = 56$ ) in the treated fiber group.....	51
32. Variations in score #1 (magnesium and calcium intensity) and score #5 (potassium, chromium, and iron intensity) are present in the treated fiber lots .....	52
33. Discriminant analysis with cross validation correctly identified differences between good and poor property treated fibers .....	53
34. Discriminant loadings show the differences in good and poor treated fibers can be attributed to primarily inorganic elements .....	53
35. Loading #1 shows a variance in PDMS concentration ( $m/z = 73, 147$ ) in the treated fiber group.....	54
36. Loading #2 shows a variance in PDMS concentration ( $m/z = 73, 147$ ) in the treated fiber group .....	55
37. Discriminant analysis with cross validation correctly identified differences between good and poor property treated fibers using organic components .....	55
38. Discriminant loadings show the differences in good and poor treated fibers .....	56
39. Relative magnesium and calcium intensities for treated fibers show that good fibers have higher cation concentration .....	57
40. Treated D1374-6A (good) fibers with calcium and magnesium overlay show an uneven distribution of cations.....	58
41. XPS survey spectra of D1374-6A, 1500 ft. good property fiber .....	59
42. XPS survey spectra of D1424-6C poor property fiber.....	59
43. Surface contour plot of D1374-6A, 1500 ft. (good property) fiber .....	61
44. Surface contour plot of D1424-6C (poor property) fiber.....	61
45. Horizontal section plot of D1374-6A, 1500 ft. (good property) fiber .....	62

46. Horizontal section plot of D1424-6C (poor property) fiber.....	62
47. Vertical section plot of D1374-6A, 1500 ft. (good property) fiber .....	63
48. Vertical section plot of D1424-6C (poor property) fiber .....	63
49. Scanning electron microscopy image of D1374-6A (good property) fiber .....	64
50. Scanning electron microscopy image of D1424-6C (poor property) fiber .....	64
51. Loading #1 shows a variance in aluminum concentration ( $m/z = 27$ ) in the variable treated group .....	65
52. Loading #2 shows a variance in elemental silicon concentration ( $m/z = 28$ ) and dialkylphthalate concentration ( $m/z = 149$ ) in the variable treated group .....	66
53. Loading #3 shows a variance in potassium concentration ( $m/z = 39$ ) and PDMS ( $m/z = 28, 73, 147$ ) in the variable treated group .....	66
54. Discriminant analysis with cross validation correctly identified differences between untreated and treated fibers .....	67
55. Discriminant loadings show differences in untreated and treated fibers can be attributed to organic components .....	68
56. Discriminant analysis with cross validation correctly identified differences between regular and high treated fibers .....	68
57. XPS survey spectra of untreated D1239-3C fiber .....	69
58. XPS survey spectra of regular treated D1239-3C fiber .....	70
59. XPS survey spectra of high treated D1239-3C fiber .....	70

## ABSTRACT

Carbon-epoxy materials are finding increased structural uses in areas such as aerospace, aeronautical, and sporting goods applications because they can be produced with desirable strength-to-weight properties. Historically, the limiting factor to the strength of those composites has been the integrity of the fiber-resin interface bond. Recently, surface analysis methods have been introduced to study this fiber/matrix interface.

In this study, SIMS, XPS, and AFM were used to characterize both untreated and electrochemically treated PAN-based carbon fibers. Hexcel Corp. provided the fibers studied and included poor quality fibers from lots with mechanical properties that failed to meet the product specification as well as fibers from good quality lots. It was hypothesized that the poor mechanical performance observed in some of the fiber lots was the result of either chemical or topographic abnormalities in the fibers. It was proposed that these abnormalities could be detected by the surface sensitive techniques mentioned.

Multivariate statistical techniques were used to explore relationships between the SIMS spectra and the mechanical test results. Principal components analysis (PCA) and discriminant analysis with cross validation were used to analyze the SIMS spectra of both treated and untreated fibers. Statistically significant differences in the surface chemistry of "good" and "poor" quality fibers were identified in both treated and untreated fibers. The PCA and discriminant loadings assisted in identifying the chemistry of changes in both inorganic and organic functionalities on the poor quality fibers. These changes include an increase of oxygen on poor property untreated fiber spectra, an increase of unsaturated hydrocarbon fragments on good property untreated fiber spectra, and differences in the amount of aluminum, PDMS, magnesium, calcium, and potassium. Treated fibers primarily differed in magnesium and calcium concentrations, as well. The resulting analysis also includes that there was an increase in nitrogen containing fragments on the spectra of poor property fibers.

Preliminary Atomic Force Microscopy analysis found differences in topography correlating to the mechanical properties; however, more work would be needed to determine whether variations are statistically significant.

## CHAPTER 1

### INTRODUCTION

Carbon and graphite materials are among the lightest refractory materials known [1, 2]. They have low density, low thermal expansion, high thermal and electrical conductivity, and are considered attractive for high-temperature applications because they maintain strength and stiffness above 2500K [2]. Because carbon fibers can be produced with desirable strength-to-weight properties, they are finding increased structural uses in areas such as aerospace, aeronautical, and sporting goods applications.

Carbon fibers are usually produced commercially with either a textile precursor such as polyacrylonitrile (PAN) or a pitch precursor [3]. The carbon fibers are woven together and used to reinforce various matrix materials including epoxy and cyanate ester resins. This reinforcement allows for improved impact strength and fracture toughness for the composite material by slowing down cracks that would otherwise propagate through the matrix and weaken the material [1, 2].

#### Problem in This Area

Historically, the strength of the fiber-resin interface bond has been found to be the limiting factor to the mechanical properties of carbon-epoxy materials [4]. Without maximum adhesion between the fiber and the matrix material, poor interlaminar shear

strength, a lack of delamination resistance, and low tensile strength all result in rendering the composite structure useless [1, 5, 6]. To optimize this adhesion between the fiber and the matrix material, the surface properties of the fiber are often electrochemically oxidized through the application of surface treatments [1, 2, 4-12]. This results in heightened dispersive interactions (London Forces), nondispersive interactions based on acid-base groups, covalent chemical bonds, and physical interactions, which all result in an increase in mechanical properties [6].

### Motivation for Research

The strength of composite structures has historically been predicted through the mechanical testing of particular matrix/fiber reinforcement combinations. These tests include, but are not limited to, tensile testing, compression testing, shear testing, fatigue testing, or a combination thereof.

It is known that many of the measured mechanical properties of composites are governed by the quality of the adhesion between the fiber and the matrix. Without suitable interfacial interaction, proper load sharing between the fibers does not take place, resulting in a weaker material [3]. Recently, surface analysis techniques have been introduced to quantify the integrity of this fiber/matrix interface and compared to current mechanical methods. It is believed that the results obtained by mechanical tests are a function of surface characteristics and can be correlated to surface analysis techniques such as x-ray photoelectron spectroscopy, secondary ion mass spectrometry, and atomic force microscopy.

### Research Objectives

The goal of this project was to explore the feasibility of using surface analysis to predict strength of carbon composite materials. Specifically, the ability of secondary ion mass spectrometry to identify differences between fibers with poor mechanical properties and good mechanical properties was explored. This objective was completed using the following procedures:

- Surface analysis methods were used to analyze poor property fibers that failed to meet product specification as well as fibers from good quality lots.
- Differences among the fiber groups and relationships between the acquired spectra and mechanical results were explored by using multivariate techniques.
- The statistical significance of differences between the poor property fibers and the good property fibers was determined.

## CHAPTER 2

### BACKGROUND

#### Analytical Methods

Carbon fibers are a challenge to study using surface sensitive techniques. Most spectroscopies are used with appropriate experimental protocol but traditional methods usually provide only the bulk information, 1000 Å or more, into the material. With chemical functionality studies, the information sought after is in the range of 1 Å to 100 Å so limited analysis techniques are available with specific advantages and disadvantages to each [1].

#### X-ray Photoelectron Spectroscopy

X-ray photoelectron spectroscopy (XPS), also known as electron spectroscopy for chemical analysis (ESCA), is the most widely used of the contemporary surface characterization methods [13]. A large amount of information is acquired from each spectrum (Table 1) and the technique is flexible enough to be used on a large variety of sample types.

Theory and Principles of the Technique. Each atom on the surface of a material (except for hydrogen) consists of valence electrons that are involved in chemical bonding

along with core electrons. These core electrons possess a unique binding energy which is characteristic of the type of atom to which it is bound. By analyzing the binding energies of the electrons and the peak areas, quantitative elemental surface analysis is possible [14].

Table 1. Information obtained by x-ray photoelectron spectroscopy from Ratner and Castner[16].

---

In the outermost 10 nm of a surface, XPS can provide:

- Identification of all elements (except H and He) present at concentrations greater than 0.1 atomic percent
  - Semiquantitative determination of the approximate elemental surface composition (error <  $\pm 10\%$ )
  - Information about the molecular environment (oxidation state, bonding atoms, etc.)
  - Information about aromatic or unsaturated structures from shake-up ( $\pi^* \rightarrow \pi$ ) transitions
  - Identification of organic groups using derivatization reactions
  - Nondestructive elemental depth profiles 10 nm into the sample and surface heterogeneity assessment using (1) angular-dependent XPS studies and (2) photoelectrons with differing escape depths
  - Destructive elemental depth profiles several hundred nanometers into the sample using ion etching (for organics)
  - Lateral variations in surface composition (spatial resolution of 8  $\mu\text{m}$  to 150  $\mu\text{m}$ , depending upon the instrument)
  - "Fingerprinting" of materials using valence band spectra and identification of bonding orbitals
  - Studies on hydrated (frozen) surfaces
-

Because the electrons can only travel a short distance through the sample without undergoing inelastic collisions resulting in a drastic loss of energy, XPS is considered to be highly surface sensitive. Usually only the upper 50 Å to 100 Å of the sample is analyzed using this technique [13].

Surface analysis by x-ray photoelectron spectroscopy begins by placing the sample in an ultra-high vacuum environment ( $\sim 10^{-10}$  torr) and then irradiating the material with a source of low-energy x-rays. If the frequency of the excitation x-rays are greater than the binding energy for each element, photoemission will occur. Schematics of the x-ray photoelectron process are seen in Figures 1 and 2 [13].

The resulting photoelectrons are emitted from the surface having a kinetic energy ( $E_k$ ) measured by a hemispheric analyzer. Using the known x-ray energy ( $h\nu$ ), the binding energy ( $E_b$ ) is calculated using the Einstein relation seen in Equation 1 [13, 15, 16] where  $\phi$  is the work function of the spectrometer.

$$E_b = h\nu - E_k - \phi \quad (1)$$

The photoelectrons are then separated according to energy, counted, and related to the atomic and molecular environment from which they were ejected. A spectrum of the number of emitted electrons versus binding energy is obtained.

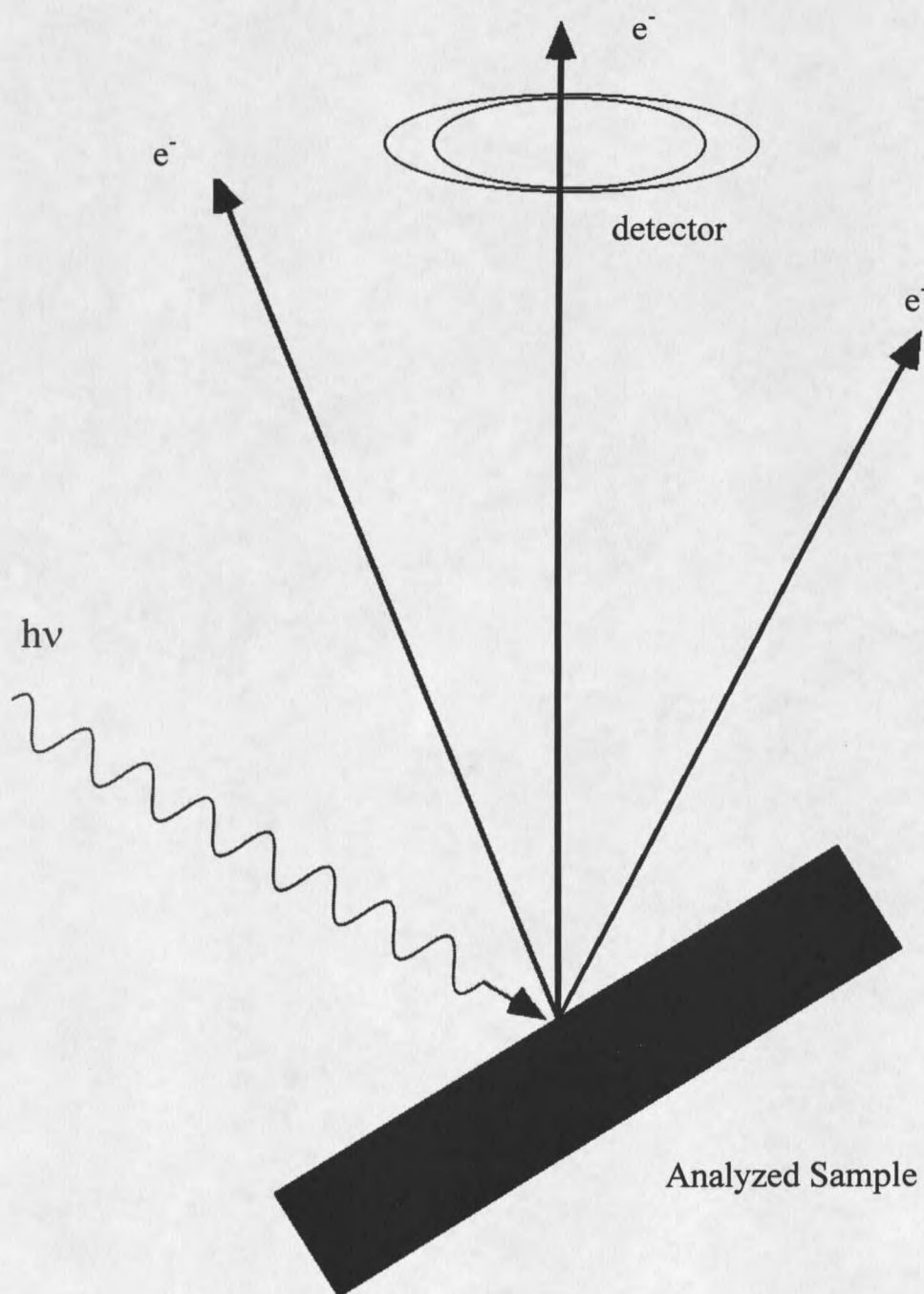


Figure 1. Schematic of x-ray photoelectron spectroscopy.

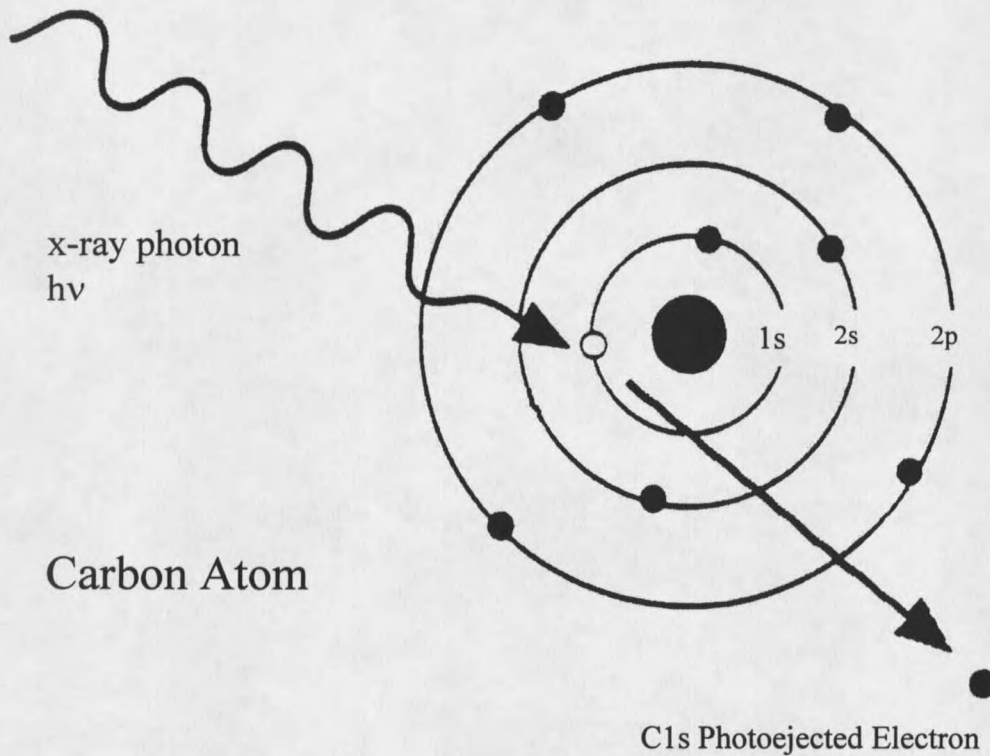


Figure 2. Schematic of a carbon atom undergoing the photoelectron process [13].

Although specific electrons of an atom have certain binding energies, the chemical environment of the atom can create variations in the values. These changes in the energy values, or chemical shifts, represent covalent or ionic bonds between atoms and help deduce the chemical structure of the material surface. Some common binding energy peak assignments for the carbon 1s peak and the oxygen 1s peak are seen in Tables 2 and 3 [13].

Table 2. Common binding energy assignments for the carbon 1s peak from Ratner and Castner [13].

<u>Functional Group</u>		<u>Binding Energy (eV)</u>
Hydrocarbon	$\underline{\text{C}}\text{-H, } \underline{\text{C}}\text{-C}$	285.0
Amine	$\underline{\text{C}}\text{-N}$	286.0
Alcohol, Ether	$\underline{\text{C}}\text{-O-H, } \underline{\text{C}}\text{-O-C}$	286.5
Carbonyl	$\underline{\text{C}}\text{=O}$	288.0
Amide	$\text{N-}\underline{\text{C}}\text{=O}$	288.2
Acid, Ester	$\text{O-}\underline{\text{C}}\text{=O}$	289.0
Urea	$\begin{array}{c} \text{O} \\    \\ \text{N-}\underline{\text{C}}\text{-N} \end{array}$	289.2
Carbamate	$\begin{array}{c} \text{O} \\    \\ \text{O-}\underline{\text{C}}\text{-N} \end{array}$	289.9
Carbonate	$\begin{array}{c} \text{O} \\    \\ \text{O-}\underline{\text{C}}\text{-O} \end{array}$	290.3

The observed binding energies will depend on the specific environment where the functional groups are located. Most ranges are  $\pm 0.2$  eV, but some can be larger.

Table 3. Common binding energy assignments for the oxygen 1s peak from Ratner and Castner [13].

<u>Functional Group</u>		<u>Binding Energy (eV)</u>
Carbonyl	$\text{C}=\underline{\text{O}}, \text{O-}\underline{\text{C}}\text{=O}$	532.2
Alcohol, Ether	$\text{C-}\underline{\text{O}}\text{-H, C-}\underline{\text{O}}\text{-C}$	532.8
Ester	$\text{C-}\underline{\text{O}}\text{-C=O}$	533.7

The observed binding energies will depend on the specific environment where the functional groups are located. Most ranges are  $\pm 0.2$  eV.

Previous Work on Carbon Fiber Surfaces. Surface analysis studies of carbon fibers using x-ray photoelectron spectroscopy were first reported in 1970. The first recorded study of XPS for the study of carbon fibers concentrated on the bulk material of the fiber in order to characterize it in relation to other forms of carbon such as graphite or diamond [9]. However, within a year of x-ray photoelectron spectroscopy's commercial use, it was found that the known increase in the electrochemical oxidation of the fiber due to the surface treatment was seen as an increased carbon-oxygen ratio using analysis techniques. The resulting chemical shifts were also noticed and this began the work in fiber treatment investigations [1, 2, 4, 5, 9, 11].

Fiber treatment investigations are usually done using one of two approaches. The first technique involves computer curve fitting programs that can estimate the proportions of carbon and oxygen groups by using the core spectrum (electron binding energies  $> 30$  eV) and the valence band spectrum (electron binding energies  $< 30$  eV). Another approach involves labeling the functional groups with a reagent that contains an element easily detectable by XPS. However, this technique is beyond the focus of this paper and will not be discussed.

The core region of an XPS spectrum is the easiest region to interpret since each type of atom has core electrons (electrons that do not play a significant role in chemical interaction) in a characteristic region, resulting in instantaneous atomic identification. Additional information about the chemical environment and subsequent chemical bonds of the atoms is then provided by core chemical shifts [1, 2]. The resolved carbon 1s and oxygen 1s regions are peak fitted to show overlapping features corresponding to different

chemical functionalities. Each region is fitted to a number of component peaks, each peak corresponding to a different surface functionality.

The valence band region, in contrast to the core region, gives peak features for all of the species present in the same region of the spectrum. This area is able to show differences that are highly sensitive to the type of material present; all the energy levels involved in chemical interaction, specific to the species studied, can be seen. Because core chemical shifts are sometimes unable to distinguish between certain subtle chemical differences, the valence band can play an important role in surface characterization [1, 2]. It must be realized, however, that valence band XPS spectra analysis requires more sophisticated calculation methods and prove that comparisons with model compounds are difficult. The resolution of the valence band spectra is also typically much lower than that of the core spectra.

Various researchers have explored the curve fitting approach with the vast majority concentrating on core spectrum studies. Over 250 papers have addressed the curve fitting area, so, only a brief description of the work that illustrates the type of information that can be provided by XPS will be mentioned here. A complete review of this material can be found in Peter Sherwood's referenced papers [1].

The previous XPS work on untreated fibers showed concentrations of oxygen and nitrogen in addition to the expected carbon in the core spectrum [1, 2, 4, 5, 9, 11, 12]. Simon, Jacobasch, Pleul, and Uhlmann attributed these traces of nitrogen to the manufacturing process and the oxygen peak to surface oxidation reactions. Jacobasch, Grundke, Uhlmann, Simon, and Mäder stated that this same oxygen and nitrogen

polarized the bonds between carbon and the heteroelements and created polar properties of the differently treated surfaces [11].

Previous work by researchers on the high resolved core carbon 1s spectrum of untreated carbon fibers showed the different bonds of carbon where the main component peak (the lowest binding energy peak) corresponded to the carbon fiber and C=C bonds. Other carbon bonds were identified by the higher binding energy features of oxidation: alcohol (C-OH), carbonyl (C=O), and carboxyl (COO) and amino C-N (Figure 3) [1, 2, 4, 11].

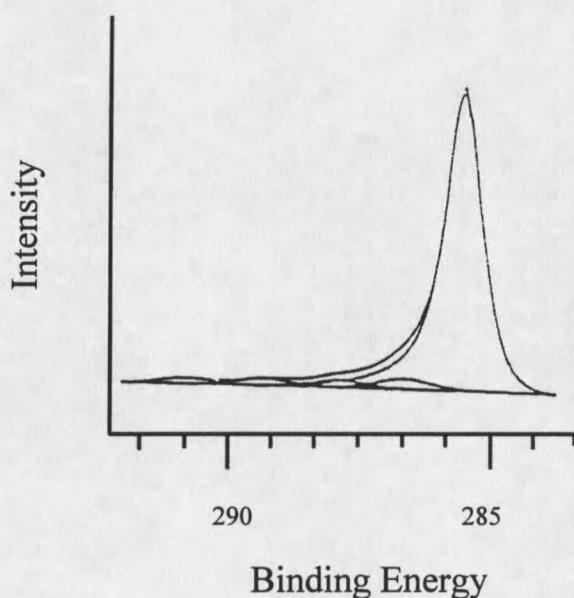


Figure 3. High resolution carbon 1s peak of untreated carbon fiber by Sherwood et al.[1].

A wide shake-up peak was also observed in the carbon 1s core spectrum that indicated conjugated delocalized  $p_{\pi}$  electrons [4]. These component peaks (shake-up peaks) in this range were a result of a charge transfer of  $\pi$  electrons from  $\pi$  orbitals to  $\pi$

orbitals. This extreme width of the shake-up range indicated an extensive  $\pi$  electron system on carbon fiber surfaces [4, 11].

After an electrochemical-oxidation surface treatment has occurred, the number of surface groups containing oxygen and nitrogen increased indicating a change in the surface composition [1,2]. A weakly increased carboxyl component peak and a strongly increased alcohol component peak were observed in the high resolved carbon 1s spectrum (Figure 4) and the atomic ratio (oxygen/carbon) increased by a factor of 1.5. In contrast, the intensity of the observed shake up peaks decreased in area by 43%. This was due to the delocalized  $\pi$  electron system of the carbon fiber surface being partially destroyed during the oxidation reaction. In the case of oxidation, alcohol groups were generated by the opening of carbon double bonds [4, 11].

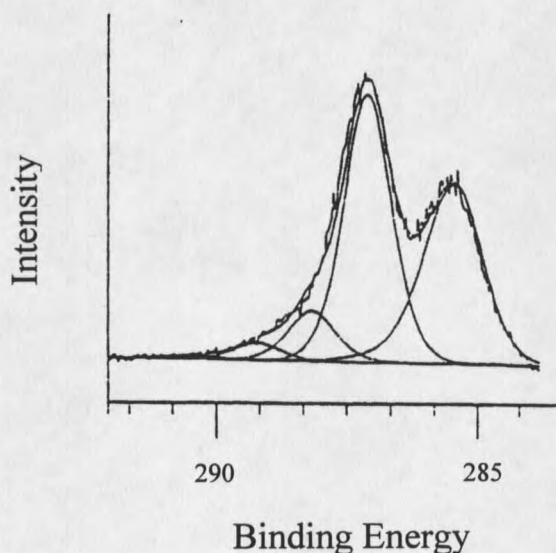


Figure 4. High resolution carbon 1s peak of surface treated carbon fiber by Sherwood et al.[1].

Some of the recent work done in carbon fiber analysis has concentrated on the presence of contaminants resulting from impure precursor material or problems in the production route [9]. The main difficulties in dealing with this type of spectra analysis (especially with fibers of industrial importance) are threefold. First, there is the difficulty in identifying unambiguously the type and distribution of functional groups which has led people to apply derivatization or labeling methods. Second, there is the lack of spatial resolution. The recent discovery of imaging XPS will significantly improve this situation, however, the current resolution limit of  $\sim 10 \mu\text{m}$  is greater than the typical carbon fiber diameter. Third, the low level of oxidation encountered is only 5% to 10 % the intensity of the main carbon 1s peak, resulting in difficult data extraction [9, 10].

### Secondary Ion Mass Spectrometry

Secondary ion mass spectrometry (SIMS) has also been used to investigate the surfaces of carbon fibers. The potential advantages of this analysis technique include the ability to identify hydrogen containing fragments, the ability to distinguish different isotopes (and therefore use isotopic labeling) and the greater sensitivity to elemental species than for XPS. There is also the ability to provide spatial information of  $\sim 0.2 \mu\text{m}$  by the use of a fine focus liquid metal ion gun and scanning imaging SIMS that can allow meaningful correlation of imaging SIMS and conventional SEM information [1, 10].

Theory and Principles of the Technique. Secondary ion mass spectrometry is based on the fact that charged atomic and molecular species are ejected from the surface of a condensed phase, such as liquid or solid, under the bombardment of high-energy

primary ions such as cesium or gallium. This analysis is performed in an ultra-high vacuum environment of  $\sim 10^{-10}$  torr similar to XPS [14, 17, 18].

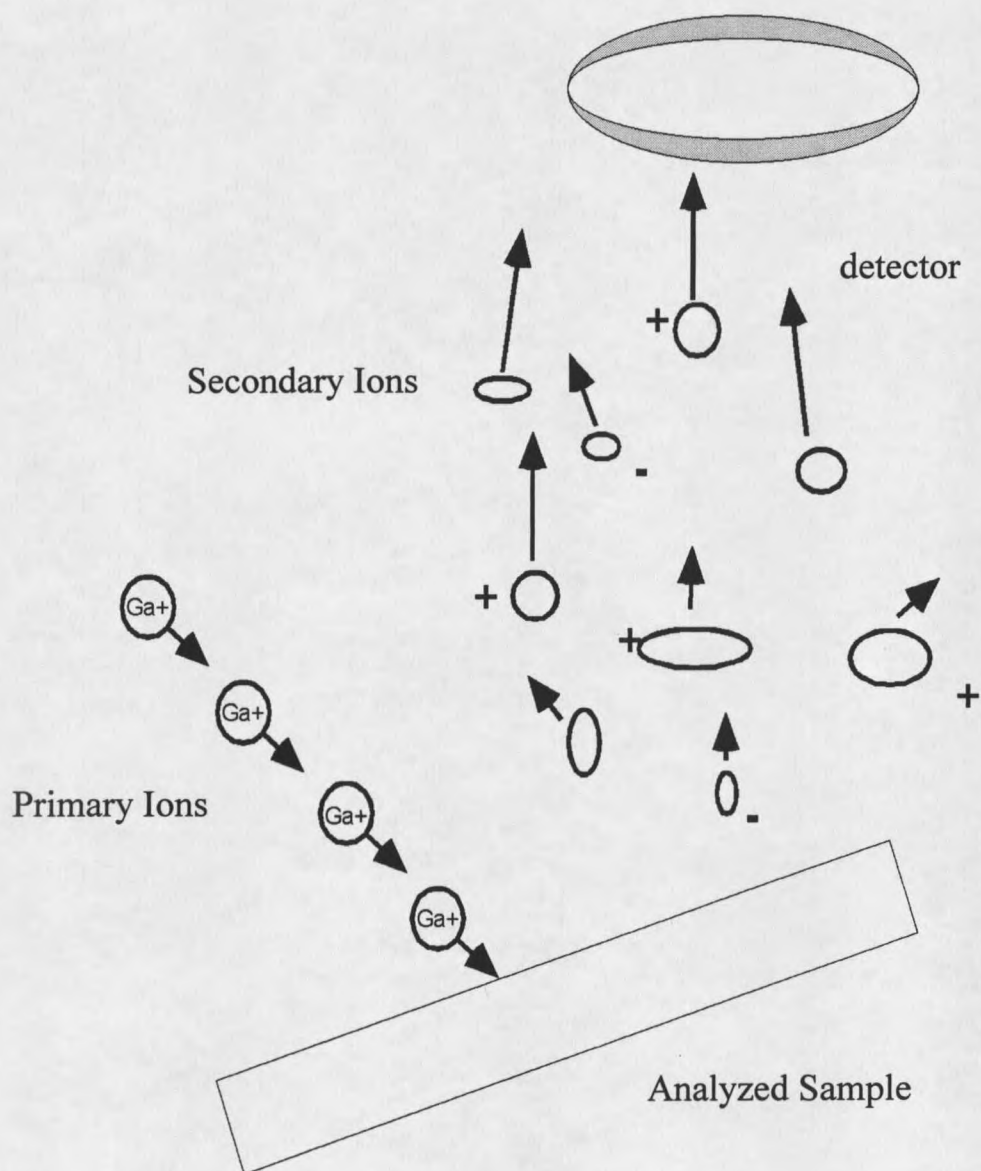


Figure 5. Schematic of secondary ion mass spectrometry.

When the bombarding primary ions transfer some of their energy to the lattice atoms and cause energy and momentum transfer around the point of impact, a cascade of atomic collisions occur [14, 17]. This results in not only a change in lattice structure but also the emission of secondary ions that can be easily mass separated by different types of mass analyzers and is used to investigate the elemental makeup of the specimen. A schematic of the SIMS process is seen in Figure 5. Because cluster ions are emitted along with elemental ions, a surface fragmentation pattern of the material is generated and the secondary ions allow the chemical structure of the surface to be studied [14].

Almost all of the secondary ions that are emitted originate from the uppermost atomic layers of the bombarded surface. Because of this, SIMS is considered to be more surface sensitive than XPS gaining information from only the top one or two monolayers of the material.

As mentioned previously, another advantage of secondary ion mass spectrometry is the capability of monolayer imaging [17, 18]. The position of the elements and ion clusters ejected from the sample surface is recorded and images consisting of either all the detected ions or only ions in a certain mass range can be mapped.

One disadvantage of secondary ion mass spectrometry in analytical application is the lack of quantification possibilities. Because different elements and cluster ions have different ionization potentials, quantification must be achieved by either semi-empirical ionization models or by the additional application of another analytical techniques such as x-ray photoelectron spectroscopy. Another disadvantage includes the "violence" of the SIMS process. Once an area of the surface has been hit by the primary ion, it is

destroyed. However, it must be remembered that under static conditions no spot on the surface is hit more than once.

Previous Work on Carbon Fiber Surfaces. Briggs's first work involving carbon fibers and SIMS illustrated the use of imaging SIMS to provide evidence of spots of thermoplastic material adhering to carbon fibers after fracture of composite materials [9]. However, this work was before the introduction of Time-of-Flight (ToF) mass spectrometry to the SIMS technique when a high rate of specimen destruction resulted in order to work at the resolution necessary to image individual fibers.

After the introduction of ToF-SIMS, Hearn and Briggs studied the surface chemistry of commercially available PAN-based fibers that were stated by the manufacturer to be either untreated or electrochemically treated [10].

The spectra obtained from the untreated fibers were found to be very irreproducible and exhibiting variations even within a single spool. However, the spectra could be rationalized completely on the basis of contributions from hydrocarbon/polyaromatic species, inorganic species, and organic contaminants. In the low mass range ( $m/z < 200$ ), the intense peaks were found to be primarily due to hydrocarbon fragments. Also observed was a peak at  $m/z = 23$  ( $\text{Na}^+$ ). In the high mass range ( $m/z = 200-500$ ), the noticeable peaks were assigned mainly to organic contaminants such as stearates, on the basis of fingerprint spectra comparison. Fibers that were treated with a 10% solution of ammonium bicarbonate in distilled water in the laboratory were also found to have spectra dominated by organic contaminants [10].

When tap water was used in the wash-baths of the electrochemical treatment, deposits of  $\text{Ca}^{2+}$  ions on the fiber surface (represented by a peak at  $m/z = 40$ ) were found. When NaCl was added to the wash-baths, an increase of sodium was seen at  $m/z = 23$ . Commercially treated fiber spectra was similar to that of the laboratory treated fiber spectra with comparable peaks at  $m/z = 23$  and 40.

Another important discovery by Hearn and Briggs was that the species identified on the surface of the carbon fibers appeared to represent a "memory" of its processing stages. The last of these stages involved the wrapping of spools in protective shrink-wrap plastic film that can contain phenolic antioxidants, phthalate plasticizers, and fatty acid/ester slip additives. Calculations showed that additive levels of 0.1% to 1.0% in the plastic could contaminate fibers throughout the entire spool. Since it is known that carbon fibers are highly absorptive, contamination by this route instead of through the process line could not be ruled out. The authors then concluded that future SIMS studies of carbon fiber surface chemistry would demand clean fibers, made and handled in such a way as to eliminate, as far as possible, the sources of contamination that would otherwise dominate the SIMS spectra [10].

### Atomic Force Microscopy

The atomic force microscope was first introduced in 1986 as a new instrument for examining the surface of insulated crystals. Although it was implied from the beginning that it had the capability of resolving single atoms, strong evidence for atomic resolution did not appear until 1993 [19, 20].

Theory and Principles of the Technique. Atomic force microscopy (AFM) is a surface analysis technique capable of imaging the topography and morphology changes of a specimen surface. Instead of monitoring changes in tunneling current like STM, AFM profiles a surface by utilizing the inter-atomic forces between an atomically sharp tip and the sample surface in either an ultra-high vacuum environment or under ambient conditions. As the tip approaches the surface, forces are exerted on the probe. This causes a small deflection on the attached cantilever beam that is proportional to the surface features on the specimen. A laser photodiode detector, as seen in Figure 6, can then easily measure this deflection [19, 20].

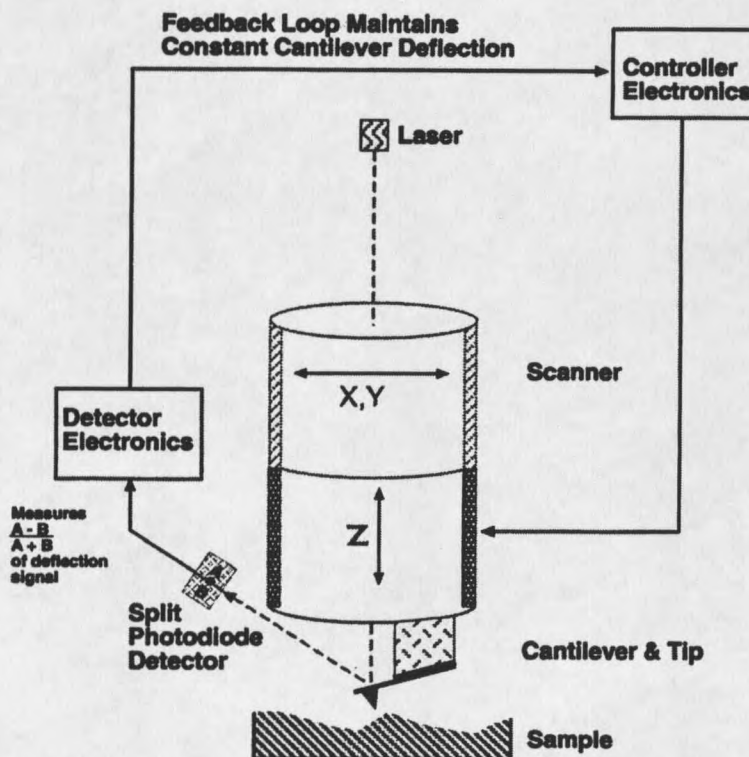


Figure 6. Schematic showing the components of contact mode atomic force microscopy [19].

In addition to the topographical information that is obtained, the AFM also calculates the force exerted on the probe tip by the use of the cantilever spring constant [19, 20].

There are three modes of the atomic force microscope: contact mode, non-contact mode, and tapping mode. The most common (and simplest) mode is the contact mode where the tip runs across the surface and is actually brought into contact with the surface and is deflected by defects in the specimen. The most common advantages and disadvantages of contact mode AFM can be seen in Table 4.

Table 4. Advantages and disadvantages of contact mode AFM from *Digital Instruments Scanning Probe Microscopy Training Notebook* [19].

---

Advantages:

- High scan speeds (throughput)
- Contact mode AFM is the only AFM technique which can obtain “atomic resolution” images
- Rough samples with extreme changes in vertical topography can sometimes be scanned more easily in contact mode

Disadvantages:

- Lateral (shear) forces can distort features in the image
  - The forces normal to the tip-sample interaction can be high in air due to capillary forces from the adsorbed fluid layer on the sample surface
  - The combination of lateral forces and high normal forces can result in reduced spatial resolution and may damage soft samples (i.e. biological samples, polymers, silicon) due to scraping between the tip and sample
-

Previous Work on Carbon Fiber Surfaces: Smiley and Delgass used atomic force microscopy to investigate the topographical changes of carbon fibers when exposed to low-temperature, low-power, oxygen plasma treatments [5]. Through their research, it was found that the grooves present in the AFM images of untreated fibers were the same as those seen by the SEM. The axial grooves were unevenly spaced from 40 nm to 120 nm apart and had a distribution of depth from 1 nm to 7 nm.

The fibers that were treated in the oxygen plasma for 2 minutes and 15 minutes were also imaged in AFM. It was found that the fiber surfaces go through an initial roughening after the short treatment, followed by an overall smoothing as treatment time was increased [5].

### Numerical Methods

Current laboratory instruments, such as secondary ion mass spectrometry instruments, are able to collect a large amount of data. One specimen can have hundreds or even thousands of measured variables. As today's chemical processes become more heavily monitored by instrumentation resulting in the collection of more data, techniques for the analysis of multivariate data by numerical means must be investigated so data will not be "wasted"[21].

### Principal Components Analysis

Principal components analysis (PCA), also known as factor analysis (FA), is a powerful tool of researchers for data compression and information extraction. PCA finds

combination of variables, or factors, that describe major trends in the data [22].

Advantages of principal components analysis can be seen in Table 5.

Table 5. Advantages of principal components analysis from Malinowski [21].

- 
- Data of great complexity can be investigated  
Principal components analysis, being a method of multivariate analysis, can deal with many factors simultaneously
  - Large quantities of data can be analyzed
  - Many types of problems can be studied  
PCA can be applied regardless of the initial lack of insight into the data; the approach can yield valuable predictions based on empirical applications
  - Data can be simplified  
Matrices can be modeled concisely with a minimum of factors, and generalizations that bring out the underlying order in the data can be obtained
  - Components can be interpreted in useful ways  
The nature of the factors can be clarified and deciphered, and data can be classified into specific categories
- 

Theory and Principles of the Technique Mathematically, PCA is “a multivariate technique for reducing matrices of data to their lowest dimensionality by the use of orthogonal factor space and transformations that yield predictions and/or recognizable factors [21].” PCA depends upon an eigenvector decomposition of the covariance matrix of the process variables. For an  $m$  by  $n$  data matrix  $\mathbf{X}$ , with each variable being a column and each sample a row, the covariance matrix is defined as

$$\text{cov}(\mathbf{X}) = (\mathbf{X}^T \mathbf{X})^{-1} \quad (2)$$

PCA then decomposes the data matrix as the sum of the outer product of vectors  $t_i$  and  $p_i$  plus a residual matrix  $E$

$$\mathbf{X} = t_1 p_1^T + t_2 p_2^T + \dots + t_k p_k^T + E \quad (3)$$

where  $k$  must be less than or equal to the smaller dimension of  $\mathbf{X}$ . Each term of this series is a principal component of the matrix. The  $p_i$  terms are known as the loadings and contain information on how the variables relate to each other. The  $t_i$  terms are projections of  $\mathbf{X}$  onto the  $p_i$  and are known as the scores matrix that represents how the samples relate to each other.

Principal components analysis of a multivariate data set can be seen graphically in Figure 7. The values of three measured variables taken from a collection of samples are plotted in three dimensions. It can be seen that the samples all lie in a plane that can be enclosed by an ellipse and that the samples vary more along one axis of the ellipse than along the other. PCA then transforms this data set into a new coordinate system, the ellipse axes, so that the major trends in the data can be captured with a minimum number of variables (principal components). The first PC describes the direction of the greatest variation in the data set (the major axis of the ellipse) while the second PC describes the next greatest amount of variation (the minor axis of the ellipse). The scores for the first

PC are the projections of the samples onto the new axis and can be interpreted as an “intensity” of the component in each sample. The loadings for the first PC are the coefficients of the equation that relates the new axis to the original variables.

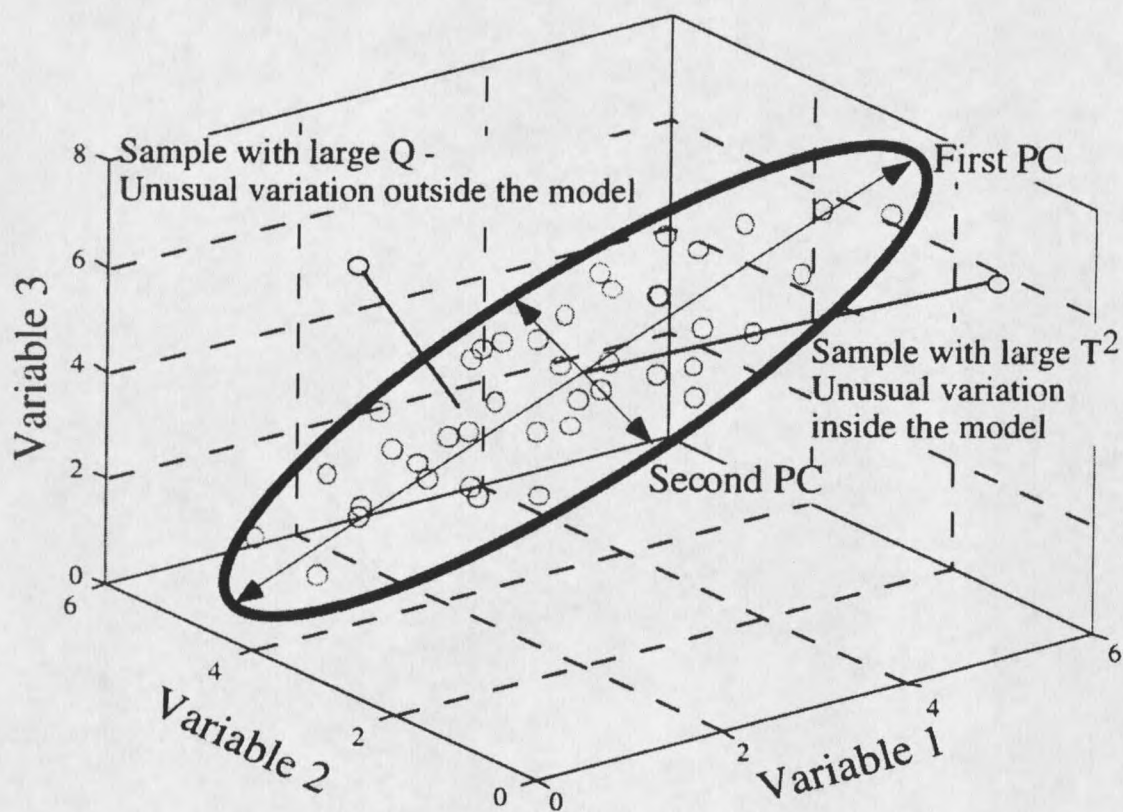


Figure 7. Graphical representation of principal components analysis [22].

In the case of SIMS work, a matrix consisting of relative peak intensities for each atomic mass unit are created for the sample size. PCA is then able to decompose this data matrix into a simpler scores matrix and a simpler loadings matrix. It is usually found that the data can be described using far fewer factors (scores and loadings) than the original variables (the number of peak intensities) without a large loss of information. It

is also found that PCA finds combinations of variables that are useful descriptions of particular phenomena [21-23].

Previous Work on Carbon Fibers. Different ways to assess quantification of fingerprint SIMS spectra can be found in the literature, however, in most of these article only a few peaks (from two to five) have been used in the analysis procedures. These selected peaks were assumed to be the only peaks directly related molecular structure of the polymers present at the surface. Unfortunately, this is not always true. With some materials, the structure of important characteristic ions cannot be learned from limited pieces of chain fragmentation alone; surface ion structure requires looking at reorganization fragments, as well. When looking at only a few peaks, often the reorganization fragments are missed.

Vanden Eynde and Bertrand found that ToF-SIMS quantification using principal components analysis on polystyrene spectra resulted in some success [24]. Unlike the semi-quantification methods previously used, multivariate techniques such as PCA allowed all of the peaks in spectrum to be analyzed. The object of this study was to test if PCA was able to discriminate between polystyrene samples with different molecular weights and end groups (*s*-butyl, *t*-butyl, *n*-butyl). It was also hoped that the molecular ions that had the strongest influence on the model could be determined. The researchers did find that the different end-groups and the low molecular weight samples were easily separated from each other in the resulting scores plots. The loadings plots also allowed the identification of the most significant contributors to the variance as well [24].

### Discriminant Function Analysis

The discriminant function is one of the most common multivariate procedures used. Simply speaking, the discriminant function allows for a reduction of the multivariate problem into a problem that involves only one variable [23].

Theory and Principles of the Technique. The discriminant function allows the researcher to find the linear combination of collected variables, which provides the maximum ratio between the mean difference of two previously defined groups to the variance within the groups. If the two groups consist of two clusters of points, the discriminant function will find the orientation of the groups where the clusters have the least scatter but separate the most. The coordinates of the axis of orientation are the linear discriminant function. This process can be seen graphically in Figure 8.

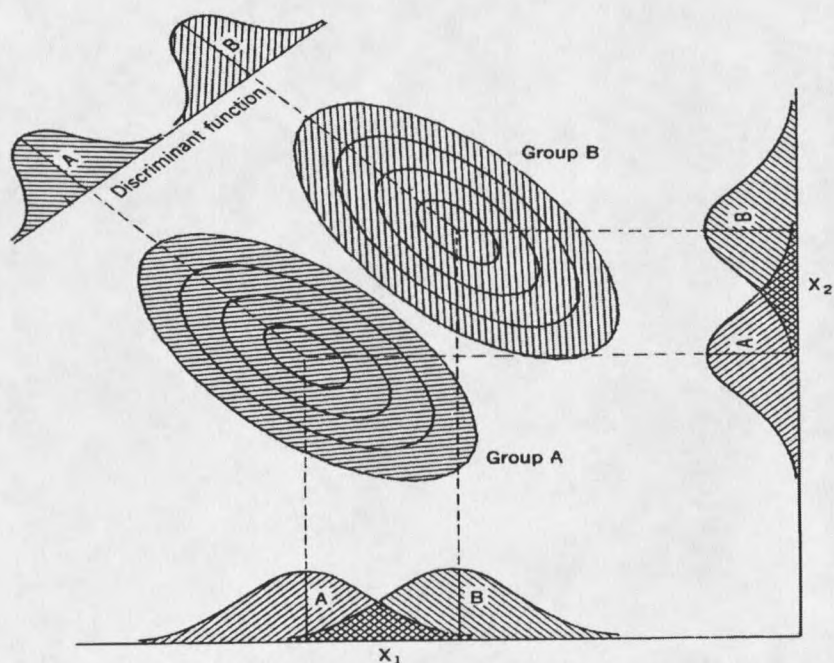


Figure 8. An illustration of the discriminant function for a two-dimensional case [23].

Once the linear discriminant function has been calculated, it can be used to assign new samples of unknown origin to one of the two original groups. This is done by putting the new sample data into the equation and locating its position along the discriminant function [23].

### Cross Validation

Using cross validation with multivariate analysis techniques allows a researcher to correlate differences to variations in individual populations and be certain that one specimen is not the principal element influencing the data.

Theory and Principles of the Technique. Cross validation consists of removing a row from the data matrix and carrying out the analysis function. The removed row is then reinserted into the matrix to see how strongly the sample affected the analysis technique. This process is repeated until every row of the data matrix has been examined [21].

## CHAPTER 3

### EXPERIMENTAL METHODS AND MATERIALS

#### Analytical Methods

All secondary ion mass spectroscopy, x-ray photoelectron spectroscopy, and atomic force microscopy work was performed at the Image and Chemical Analysis Laboratory at Montana State University, Bozeman, Montana.

#### SIMS Analysis

Hexcel manufactured all carbon fibers at their establishment in Salt Lake City, Utah. The spools of fibers were then categorized into three specific groups to be compared. The first contained all untreated fibers including lots D1374-6A, D1390-6A, and R128. The second group included surface treated fibers, lots D1374-6A, D1390-6A, D1234-6A, and D1424-6C. The last group of samples contained fibers from one lot only, D1239-3C. The difference between the fibers in this group was limited to the amount of surface treatment applied to the fiber; no other process variables were changed. A brief description of the fiber lot mechanical properties can be seen in Table 6. A complete listing of the sample identification labels, fiber types, lot numbers, treatments, sample location when applicable, and other distinguishing characteristics can be seen in Appendix A.

Table 6. Fiber lot mechanical property descriptions.

<u>Lot Number</u>	<u>Tensile Strength</u>	<u>Laminate Strength</u>	<u>Property Categorization</u>
D1374-6A	787 ksi	~	Good
D1390-6A	780 ksi	~	Good
R128-04	689 ksi	~	Good
R128-06	463 ksi	~	Poor
R128-08	626 ksi	~	Poor
D1234-6A	550 ksi	~	Poor
D1424-6C	~	Failed in 0 degree	Poor
D1239-3C	807 ksi	~	Good

The first step in the experimental procedure was to prevent unwanted surface contamination by removing the outside few meters of fiber on each spool before sampling began. Six 1cm samples were cut from each spool, individually labeled, and bound on both ends with masking tape to avoid all chances of “escaping” in the high voltage, ultra high vacuum environment.

The sample was placed into the sample holder of the instrument behind an aluminum mask with a 10 mm by 1 mm slit cut out. A piece of silicon and an aluminum disk backed the fiber “bundle”. Prior to mounting, the mask, silicon, and all sample holder accessories had all been sonicated in both a hexane (HPLC grade) bath and

methanol (HPLC grade) bath and air-dried. The holder was placed into the vacuum chamber at a base pressure of  $\sim 10^{-7}$  torr.

Time-of-Flight secondary ion mass spectrometry analyses were performed using a Charles Evans & Associates ToF-SIMS instrument. By using a ToF (Time-of-Flight) analyzer instead of an alternative detector, a much greater number of ions could be acquired ( $\sim 30\%$ ) and simultaneous detection of all ions could take place. The difference in sensitivity of a time-of-flight analyzer when compared to a quadrupole analyzer can be 100 to 1000 times or more [14].

The primary ion used in analysis was a microfocused, pulsed liquid metal ion gun (LMIG) Ga<sup>+</sup> source operating at 600 pA dc at +15keV relative to ground. Because of the conducting nature of the carbon fibers, charge compensation was not needed. An 80  $\mu\text{m}$  by 80  $\mu\text{m}$  area was scatter rastered and the acquisition time for each positive ion spectra was approximately 10 minutes. Although the mass resolution was compromised to some extent by the fact that the fiber surfaces were not flat, in the low mass regions the resulting mass resolution, ranging from 2000 to 3500, was sufficient enough to distinguish inorganic from organic ions. The low mass locale has been found to contain the important information relating to chemical and structural aspects of the material so in this study, mass information above 150 atomic mass units was disregarded [17]. Complete SIMS spectra for each sample (0 to 150 atomic mass units) can be seen in Appendix B.

The SIMS spectra were imported into the MATLAB<sup>TM</sup> ToFPak Data Reduction Software, version V2.0A. Using the peak-fitting program, secondary ion peaks were

integrated for each spectrum. From atomic mass 0 to atomic mass 50, inorganic peak areas and organic peak areas were integrated separately; from atomic mass 51 to atomic mass 150, each nominal mass peak area was integrated as a single unit. The intensity values for each spectrum were imported into a spreadsheet program and a matrix with columns corresponding to the different spectra and rows corresponding to the different ion structure intensities was created for each specific group.

In secondary ion mass spectrometry work, sodium is a common surface contaminant, ionizes easily in the SIMS environment, and is present in the bulk carbon fiber in amounts of approximately 11 parts per million [25]. After running preliminary spectra, it was found that the amount of sodium was not correlated to the mechanical properties of the fibers and therefore, inorganic atomic mass unit 23 was neglected entirely from further data analysis. The values were then normalized to the total spectrum intensity to allow for a quantitative comparison between the specimens by eliminating the systematic differences in the absolute spectral intensities that might have been due to slight differences in the instrument settings. Complete matrices of the peak areas for all analyzed spectra can be seen in Appendix C.

### XPS Analysis

X-ray photoelectron spectroscopy spectra were obtained from a Physical Electronics Instrument Model 5600 spectrometer. The fiber tows were mounted on the sample holder using double-sided adhesive tape, covered with an aluminum mask, and placed into the vacuum chamber at a pressure of  $\sim 10^{-8}$  torr. An 800  $\mu\text{m}$  diameter area was analyzed using a monochromatized 0.2 mm aluminum  $K\alpha$  x-ray source at 300 watts

and pass energies of 11.75 eV (survey scans) and 58.7 eV (elemental composition peaks). The spectrum binding energy scale was calibrated by setting the CH peak maximum in the carbon 1s spectrum to 285.0 eV [13]. A survey scan from 0 to 1400 eV was acquired for each sample and the elemental composition of the fiber's surface was calculated using the instrument software based on peak areas from the carbon 1s, oxygen 1s, nitrogen 1s, calcium 1s, silicon 1s, sodium 1s, and magnesium 3p regions.

### AFM Analysis

Atomic force microscopy was performed using a Digital Instruments Dimension 3100 Series Scanning Probe Microscope in contact mode AFM. A single fiber was mounted on double-sided conducting adhesive tape and an area of 0.5  $\mu\text{m}$  by 0.5  $\mu\text{m}$  was imaged under ambient conditions. A silicon nitride probe with a spring constant of 0.12 N/m moved transversely to the fiber.

### Numerical Methods

The matrices of SIMS data were imported into MATLAB™ where they were log scaled, transposed, and mean centered using the PLS\_Toolbox program addition for eigenvector technologies. Principal components analysis was performed and scores and loadings for the different data sets were obtained.

Cross validation and discriminant analysis was performed on the original data matrix using MATLAB™ programs written by Dr. Bonnie Tyler and can be seen in Appendix D.

## CHAPTER 4

### RESULTS

Surface analysis was performed on all treated and untreated fibers. All tested specimens had not been sized. As mentioned in Chapter 3, these spools were broken into three groups; untreated fibers with either “good” or “poor” mechanical properties, electrochemically surface treated fibers with either “good” or “poor” mechanical properties, and fibers consisting of variably treated specimens. A review of the fiber groups and identification can be seen in Appendix A.

#### Untreated Fiber Spools

The first group of fibers that were analyzed and compared were the untreated good property fibers (tensile strength greater than 650 ksi) and the untreated poor property fibers (low tensile strength and/or poor laminate results). This included untreated D1374-6A and untreated D1390-6A spools along with the pilot line R128-04, R128-06, and R128-08 spools. Mechanical testing results for these fibers determining whether the fiber specimens were classified as good or poor were provided by Hexcel and can be seen in Appendix A.

### Secondary Ion Mass Spectrometry

SIMS analysis was done on each sample and the matrix of peak intensities in the low mass fingerprint region (0 through 150 atomic mass units) was created. Principal component analysis, discriminant analysis, and cross validation was then done using the spectra matrices following the experimental procedure previously described.

The main factor contributing to variability among the untreated fiber specimens was obtained by looking at the PC loading vs. atomic mass unit plots (Figures 9 through 11). From Figure 9, it was seen that the amount of aluminum ( $m/z = 27$ ) was the principal component adding the most variance within the untreated samples; the first loading had a dominant negative peak at  $m/z = 27$ . Polydimethylsiloxane (PDMS) was recognized by its strong loading peaks in Figure 10 ( $m/z = 28, 73, 147$ ) and was considered to be the second major contributor. This was not considered unusual because PDMS is a common contaminant found on the surfaces of many materials. Siloxanes are often used as lubricants or release agents in manufacturing process lines and if it is present in the material, even in small amounts, it will find its way out of the bulk material and form a thin surface layer. The ionization potential for polydimethylsiloxane in SIMS analysis is also very high resulting in common fragmentation [26, 27]. Additional loading peaks due to inorganic species such as magnesium ( $m/z=24$ ), potassium ( $m/z=39$ ) and calcium ( $m/z=40$ ) were seen in Figure 11 and were found to supply the next highest amount of variance. Unidentifiable organics were other sources of variability found when looking at higher loadings, however, the first three principal components did represent over 85%

of the total variance in the sample group and were considered to be the most important factors.

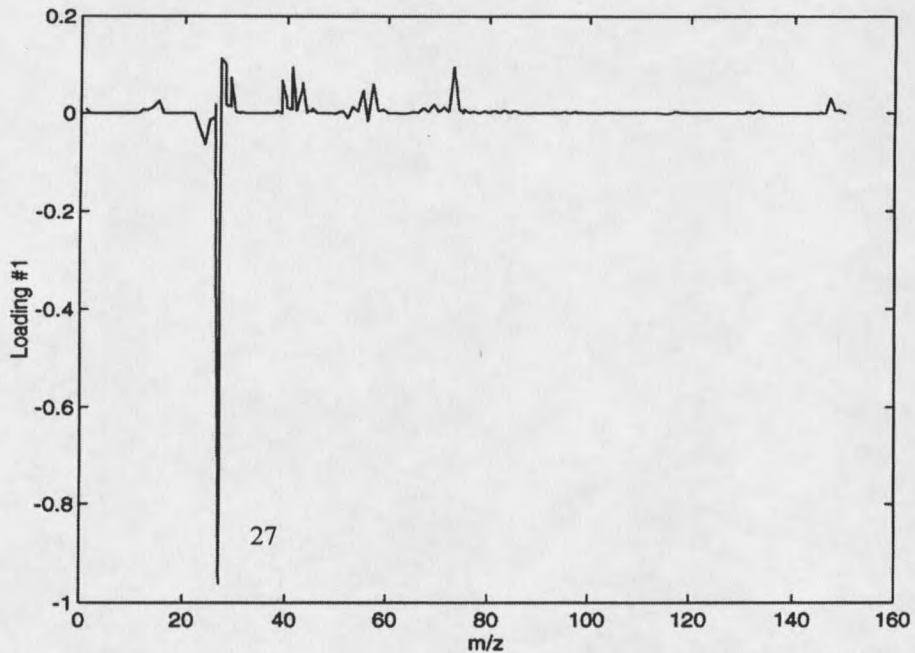


Figure 9. Loading #1 shows a variance in aluminum concentration ( $m/z = 27$ ) in the untreated fiber group.

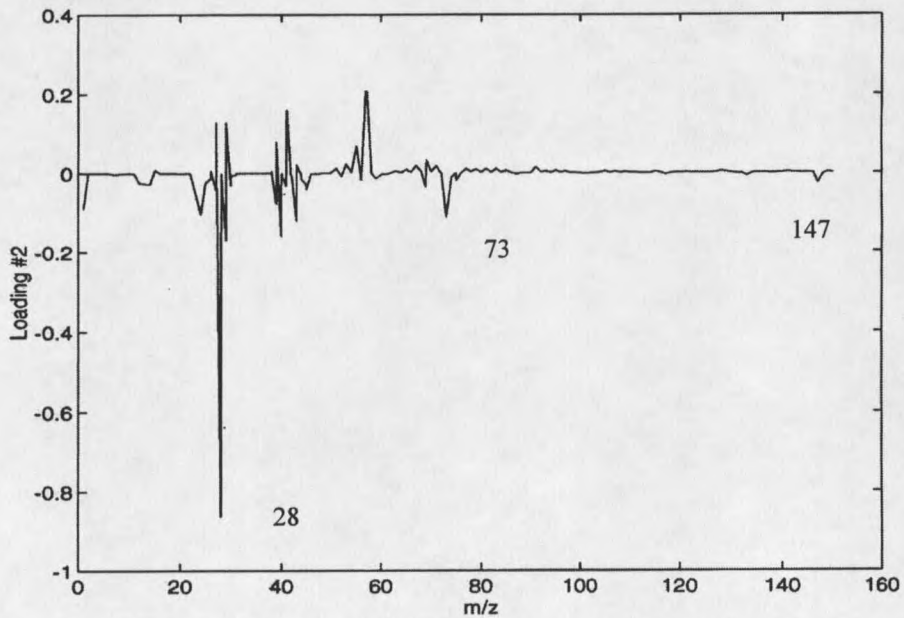


Figure 10. Loading #2 shows a variance in PDMS concentration ( $m/z = 28, 73, 147$ ) in the untreated fiber group.

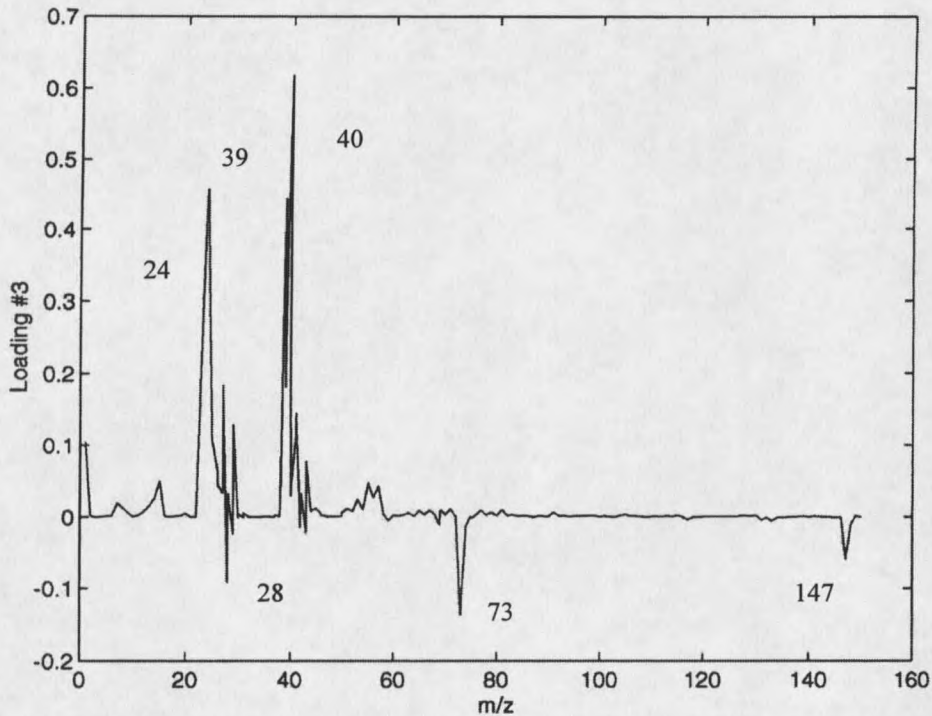


Figure 11. Loading #3 shows a variance in magnesium concentration ( $m/z = 24$ ), potassium concentration ( $m/z = 39$ ), calcium concentration ( $m/z = 40$ ), and PDMS concentration ( $m/z = 28, 73, 147$ ) in the untreated fiber group.

To explore whether the variation amongst the sample group could be correlated to the different fiber lots and the corresponding mechanical properties of the fibers, the principal component scores were examined. Variation between good and poor fibers could not be seen while looking at individual score values separately, so discriminant analysis and cross validation was done to find combined score values. The average good score value and the average poor score value was then calculated and weighted by the respective populations' standard deviation to find a weighted average value. This value was then plotted as a line on the total score versus sample number graph with the untreated samples. It was found that this number was able to separate the good and poor

property samples, represented by '+' and 'o' respectively, when 25 principal component scores were combined (Figure 12). The calculated F value of 9.4 and a confidence level of 99.9% between the two groups validated the significant difference between good and poor sample populations and can be seen in Table 9.

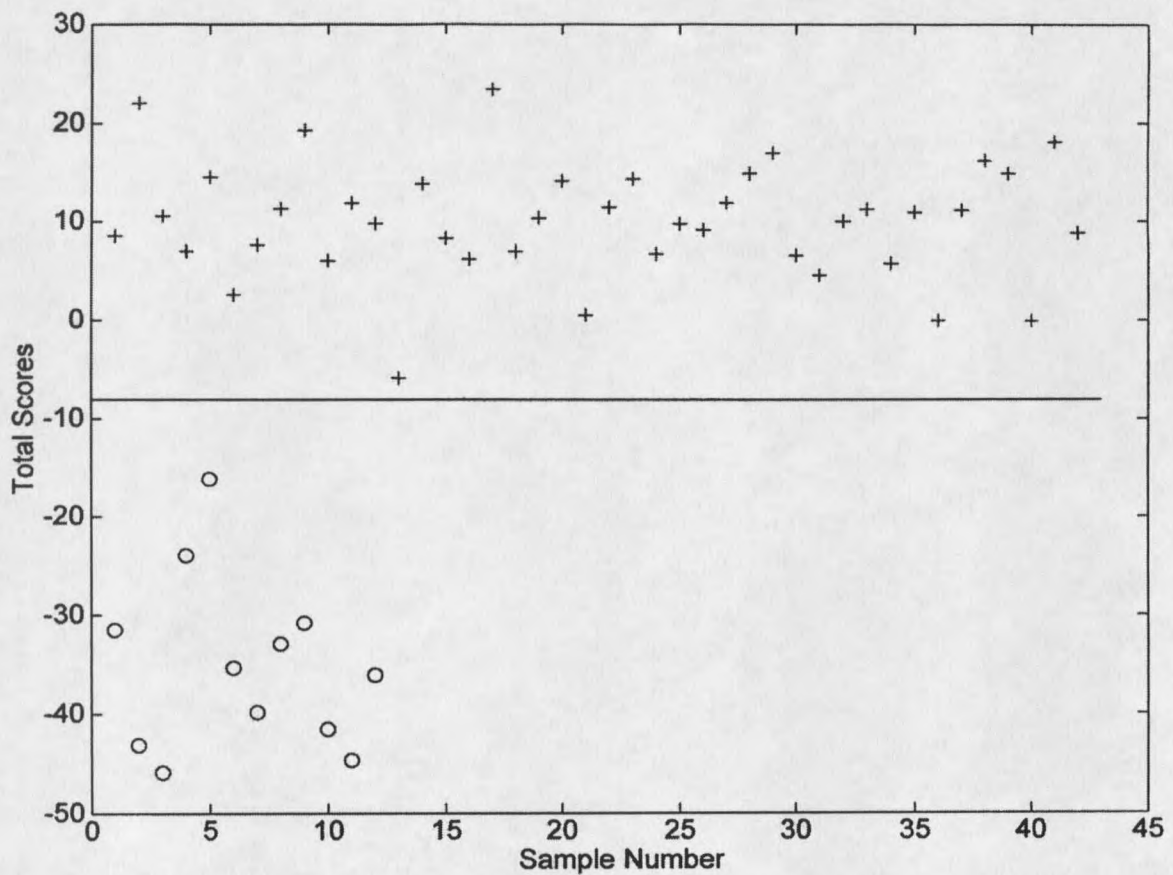


Figure 12. Discriminant analysis with cross validation correctly identified differences between good and poor property untreated fibers.

The corresponding loadings for the 25 principal components and appropriately assigned  $m/z$  values, representing the atomic elements and compounds that vary in the sample set and separate the good and poor specimens, can be seen in Figure 13. Looking at this plot, it can be seen that the loading peaks (the main source of variation between the separated groups) are attributed to be essentially all organic compounds. Unfortunately, most can not be attributed to a specific chemical compound but only as part of the carbon fiber fragments, graphitic structure segments, and oxidized fiber pieces (see Appendix E).

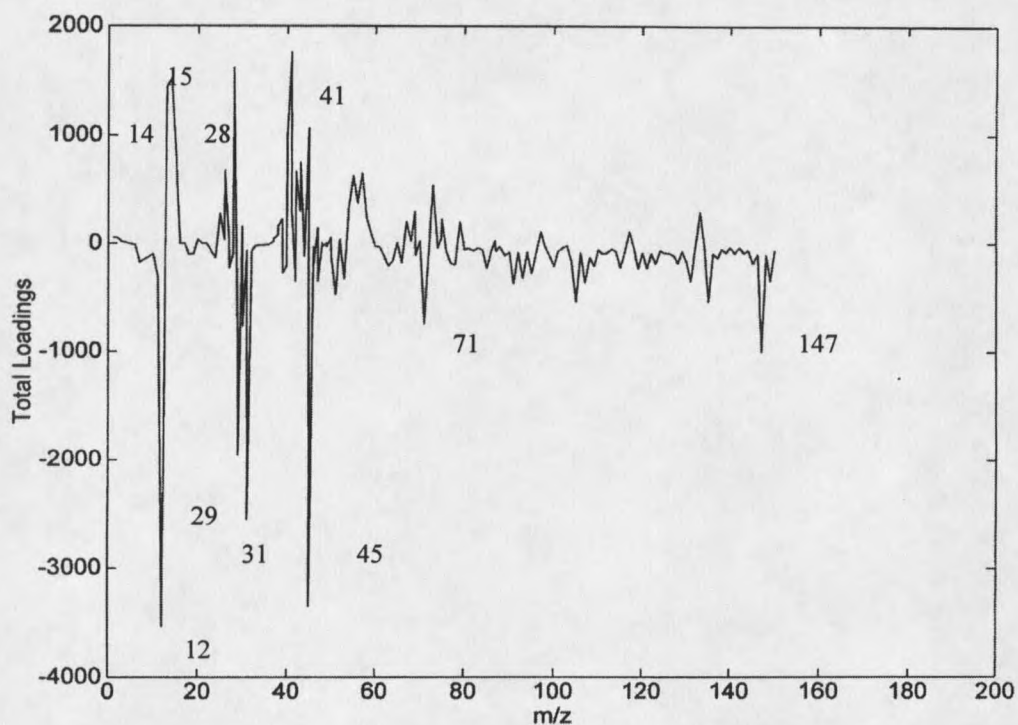


Figure 13. Discriminant loadings show the differences in good and poor untreated fibers can be attributed to organic components.

When looking only at the organic peaks of the untreated spectra to investigate differences closer, PDMS was the lone identifiable component of separation (Figure 14).

Note the strong negative loading peaks at  $m/z = 73$  and  $m/z = 147$ , characteristic of the common contaminant.

The weighted mean average value separated the good and poor samples using the scores of 20 principal components, as seen in Figure 15, with an F value of 6.4 and a confidence level of 99.9% (Table 9), strongly validated the difference between groups. The loadings and their appropriate  $m/z$  designations creating the good and poor differences can be seen in Figure 16. By looking at this loading plot, it can be seen that the poor property fibers do contain more oxygen containing fragments and saturated hydrocarbon pieces than the good property fibers before the surface treatment process even occurs. Possible fragment assignments can be seen in Appendix E.

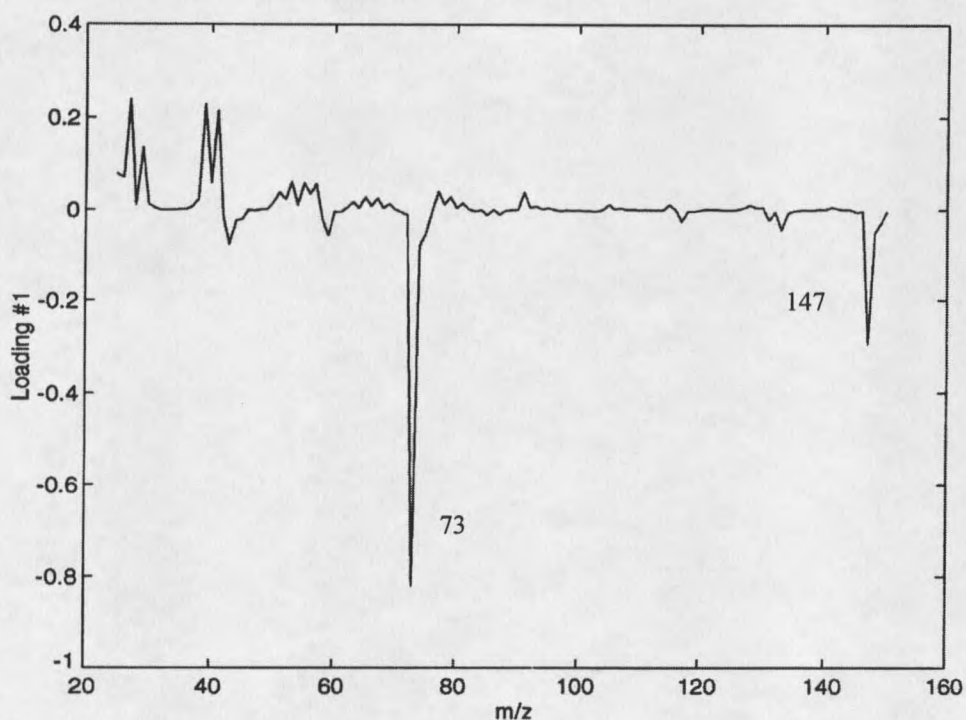


Figure 14. Loading #1 shows a variance in PDMS concentration ( $m/z = 73, 147$ ) in the untreated fiber group.

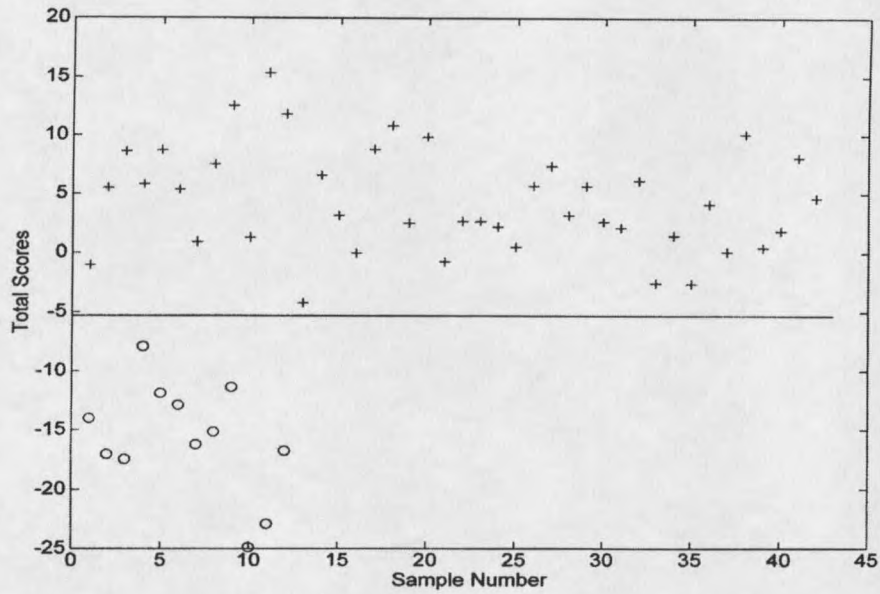


Figure 15. Discriminant analysis with cross validation correctly identified differences between good and poor property untreated fibers using organic components.

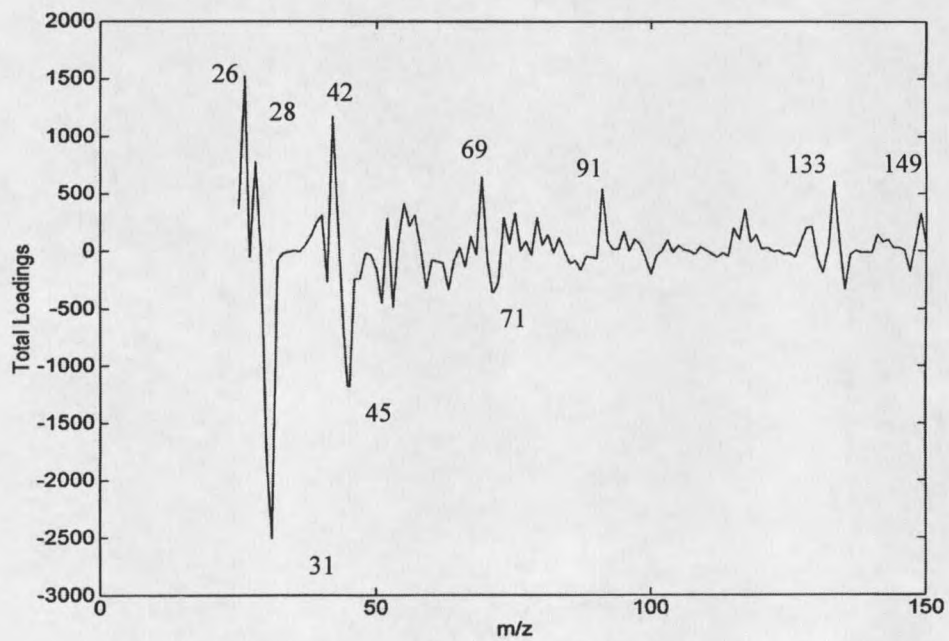


Figure 16. Discriminant loadings show the differences in good and poor untreated fibers. The spectra for poor fibers have more oxygen containing fragments and fewer fragments indicative of unsaturated hydrocarbons.

Although PDMS was the only identifiable component that separated the organic peaks, it was found that the good and poor property could still be separated using 19 principal components even with the omission of the  $m/z = 73$  and  $m/z = 147$  peaks (Figures 17 and 18). This confirms that there are other organic differences between the two types of samples other than polydimethylsiloxane, including oxidized hydrocarbons, saturated hydrocarbons, and unsaturated hydrocarbons (Appendix E). However, without increasing the mass resolution of the spectra, only low molecular weight fragments can be identified.

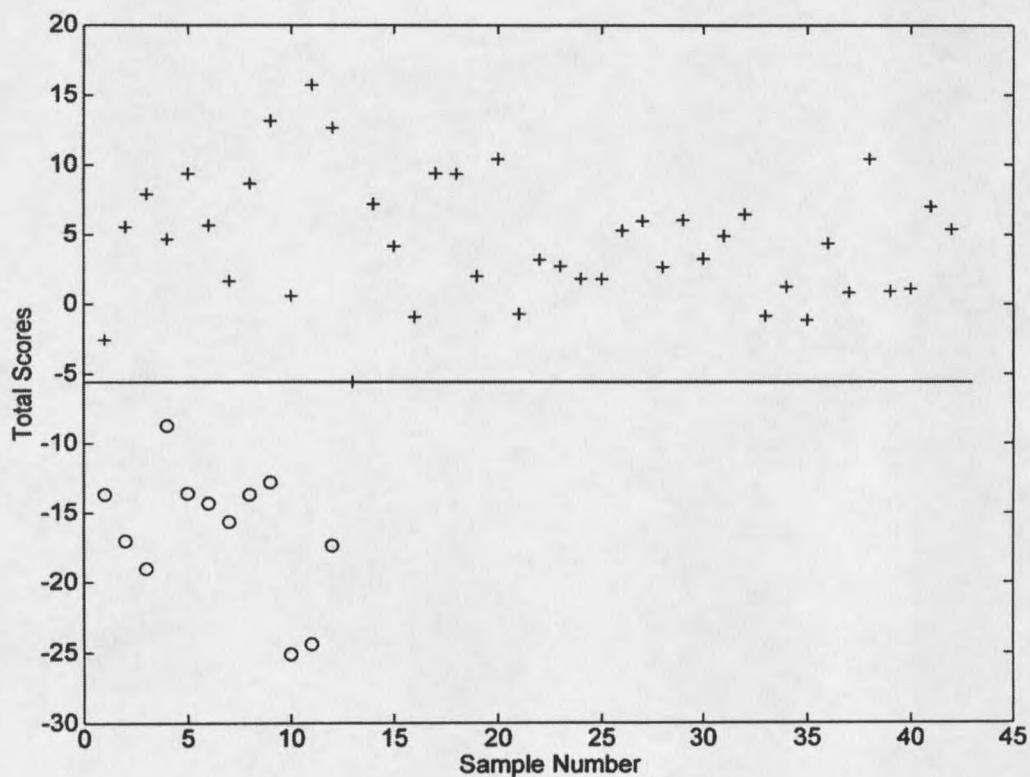


Figure 17. Discriminant analysis with cross validation correctly identified differences between good and poor property untreated fibers using organic components in the absence of PDMS.

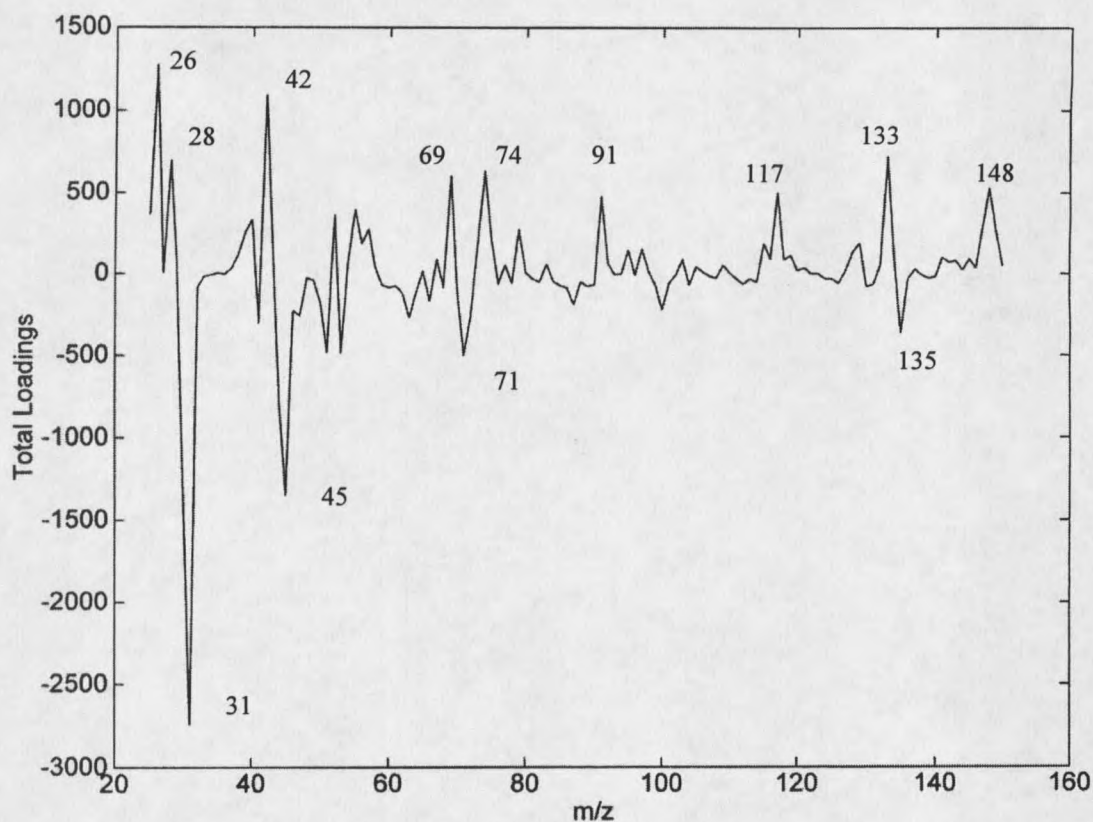


Figure 18. Discriminant loadings show organic differences between good and poor property untreated fibers can be attributed to organics other than PDMS.

### Atomic Force Microscopy

Initial topographical studies of a good baseline untreated fiber (R128-04) and a poor untreated fiber (R128-08) were done using AFM to see if surface differences between the two specimens could be seen and if a correlation to the mechanical properties could be found.

A surface contour plot of the fiber,  $0.5\ \mu\text{m}$  by  $0.5\ \mu\text{m}$ , along with a vertical section plot (along the length of the fiber) and a horizontal section plot (transverse to the

fiber) for both samples is shown in Figures 19 through 24. In Figure 19, ridges can be seen down the length of the fiber R128-04. The sizes of the ridges do vary slightly and the edge contours do not appear to be consistent. While looking at the section plots (Figures 21 and 23) it can be noted that the ridges vary in height of up to approximately 8.1 nm on this good specimen, but appear to be much less inconsistent along the length of the fiber. The striations of R128-08 tend to be covered by bumps on the fiber surface (Figure 20). These bumps do not appear to have a regular pattern, but by looking at the section plots (Figures 22 and 24) they look as if they have approximately the same diameter as the ridges on the R128-04 fiber.

When comparing the AFM images to the more common Scanning Electron Microscopy (SEM) images of R128-04 (Figure 25) and R128-08 (Figure 26), it is noticed that the same ridges and raised defects on the fiber surface are present in both sets (although image reproductions may make SEM feature identification difficult). It is evident, however, that the AFM images do permit a much closer look of the fiber and allow for quantitative height measurements to be made on each peculiarity.

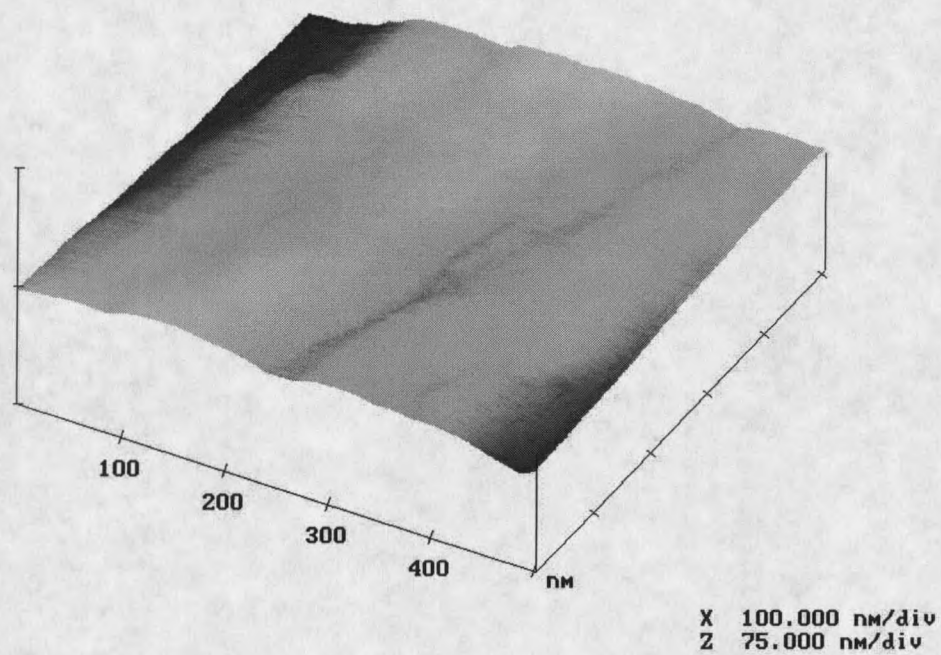


Figure 19. Surface contour plot of R128-04 (good property) fiber.

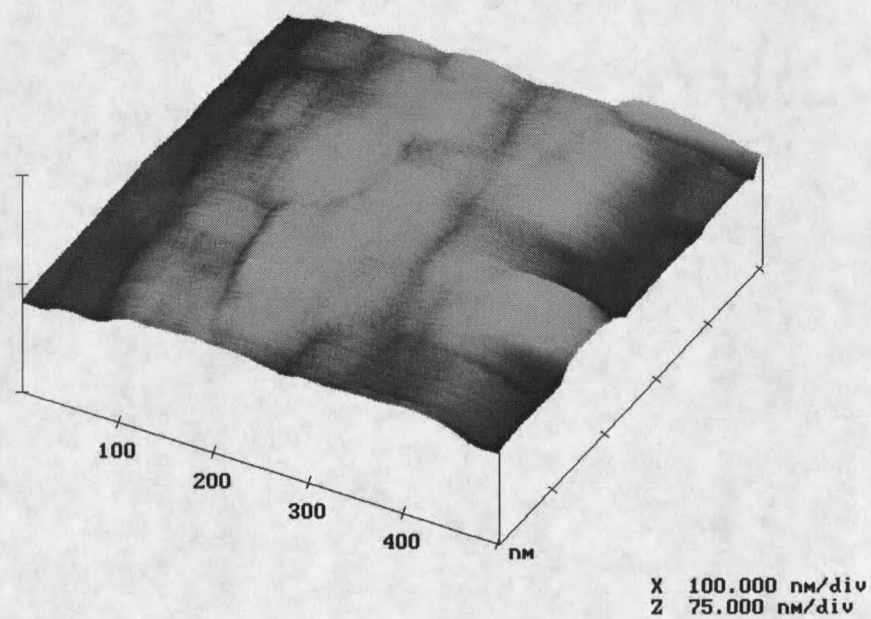


Figure 20. Surface contour plot of R128-08 (poor property) fiber.

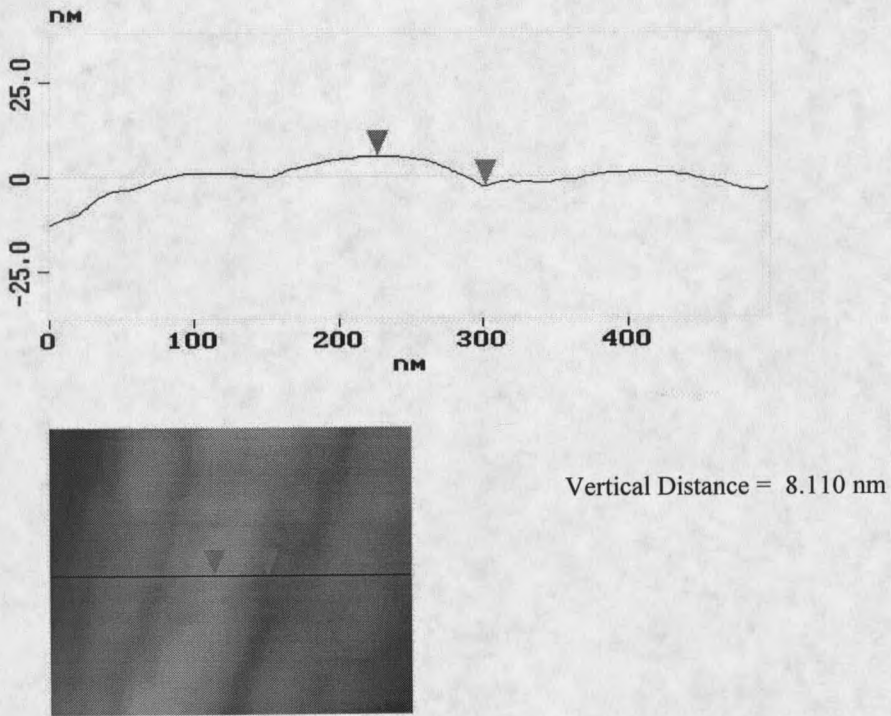


Figure 21. Horizontal section plot of R128-04 (good property) fiber.

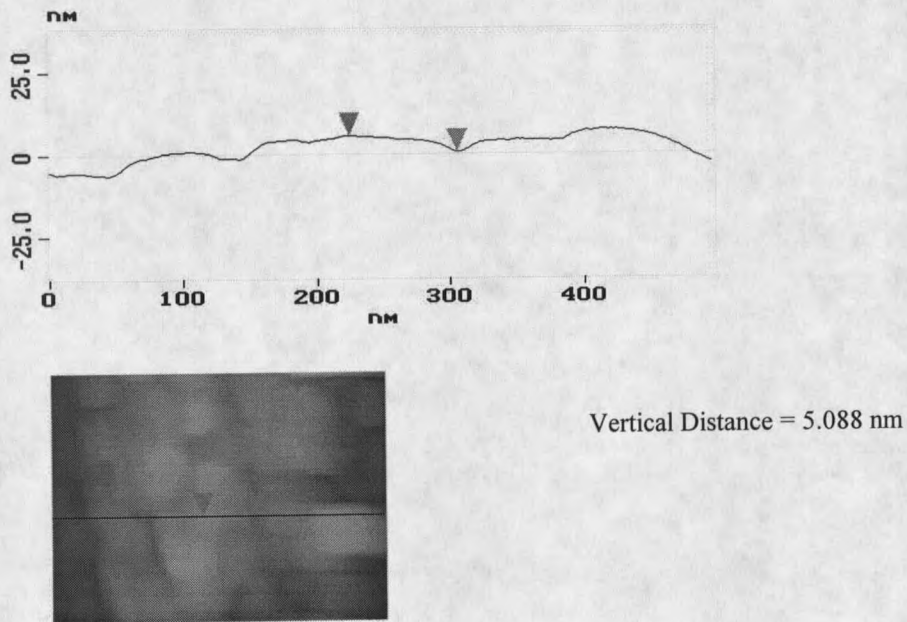


Figure 22. Horizontal section plot of R128-08 (poor property) fiber.

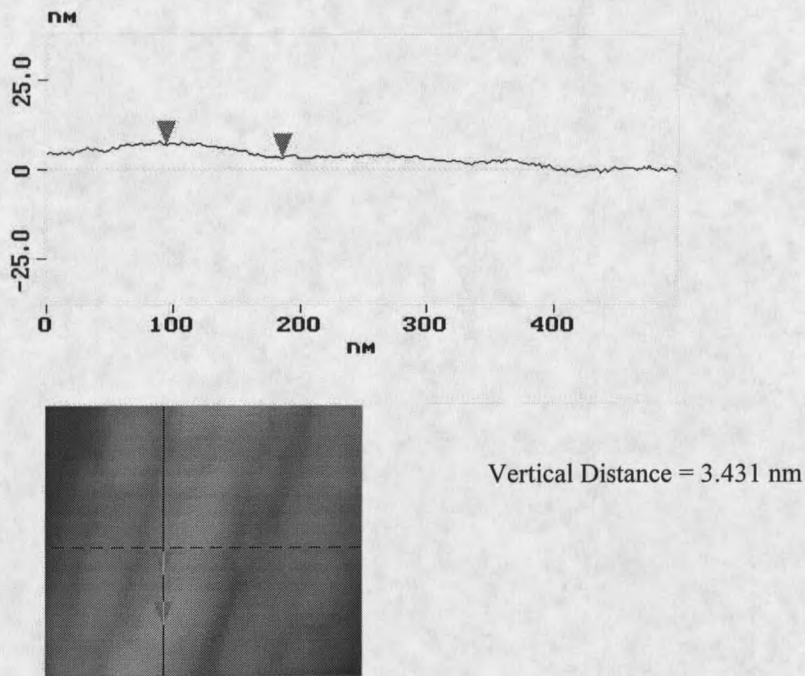


Figure 23. Vertical section plot of R128-04 (good property) fiber.

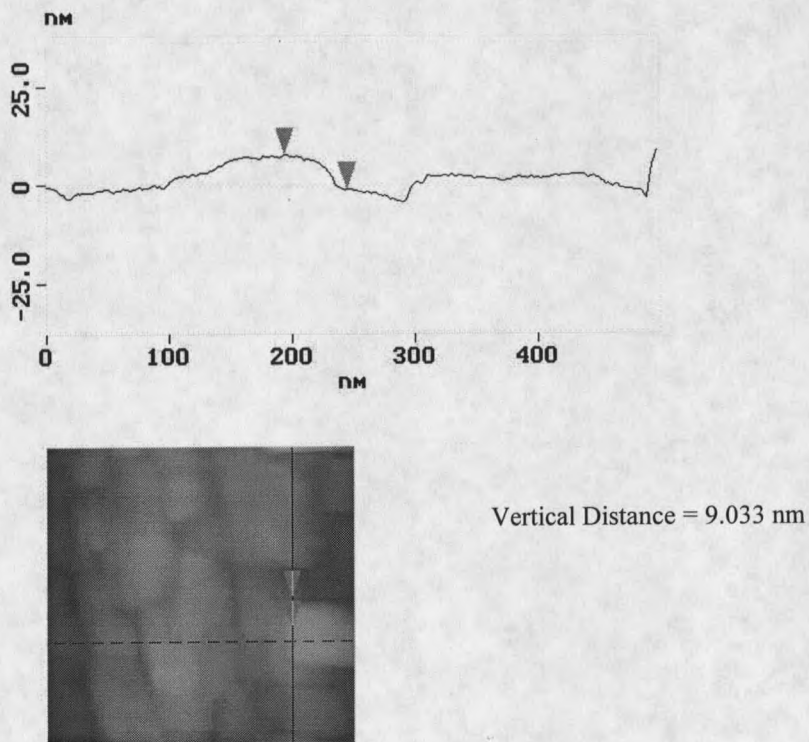


Figure 24. Vertical section plot of R128-08 (poor property) fiber.

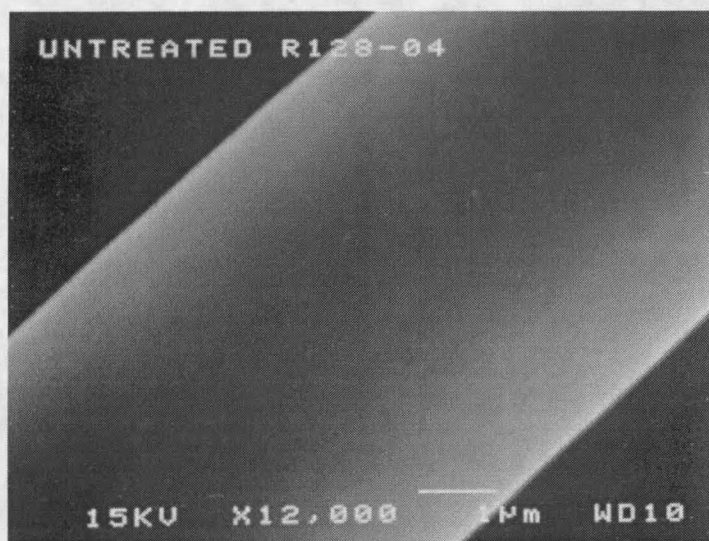


Figure 25. Scanning electron microscope image of R128-04 (good property) fiber.

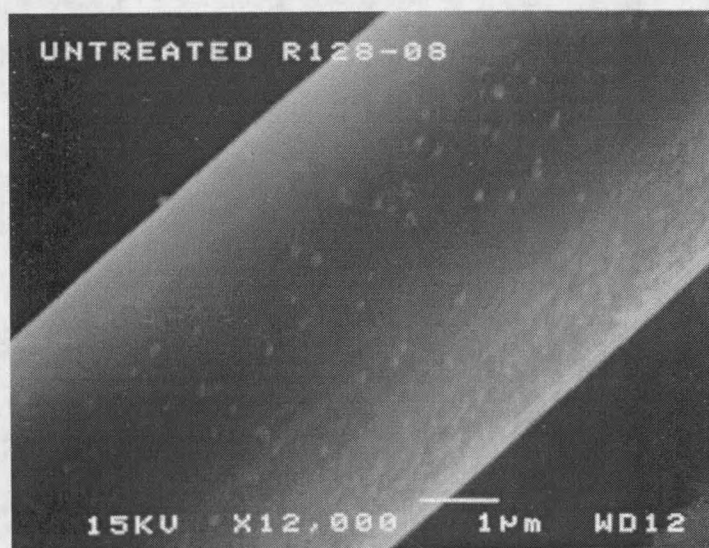


Figure 26. Scanning electron microscope image of R128-08 (poor property) fiber.

### Treated Fiber Spools

The surface treated fiber samples consisted of both good and poor property fibers including the treated D1374-6A good spools, the treated D1390-6A good spools, the D1234-6A poor spools, and the D1424-C poor spool. Tensile strength results and additional laminate results (if available) used to classify good and poor specimens can be seen in Appendix A.

### Secondary Ion Mass Spectrometry

SIMS analysis (neglecting elemental sodium ions), creation of a peak intensity matrix, principal component analysis, discriminant analysis, and cross validation were then performed according to the experimental procedure.

This sample group attributed most of its variability to the inorganic elements magnesium ( $m/z = 24$ ) and calcium ( $m/z = 40$ ) as seen as prominent positive peaks in Figure 27. From Figure 28, the dominant negative loading peak at  $m/z = 27$  showed that aluminum was responsible for a high amount of variability in principal component number 2 while PDMS ( $m/z = 28, 73, 147$ ) was clearly a major portion of the third principal component as represented in Figure 29. Loading number 4 (Figure 30) was characteristic of potassium ( $m/z = 39$ ) and PDMS ( $m/z = 28, 73, 147$ ) while potassium, chromium ( $m/z = 52$ ), and iron ( $m/z = 56$ ) were seen as strong atomic mass units in the loading number 5 plot (Figure 31). Higher loadings were considered to be due to various insignificant organic compounds and not believed to contribute much difference to the sample group. This conclusion was reached after calculating that loadings 1 through 5 represented 93% of the total variability with the surface treated samples.

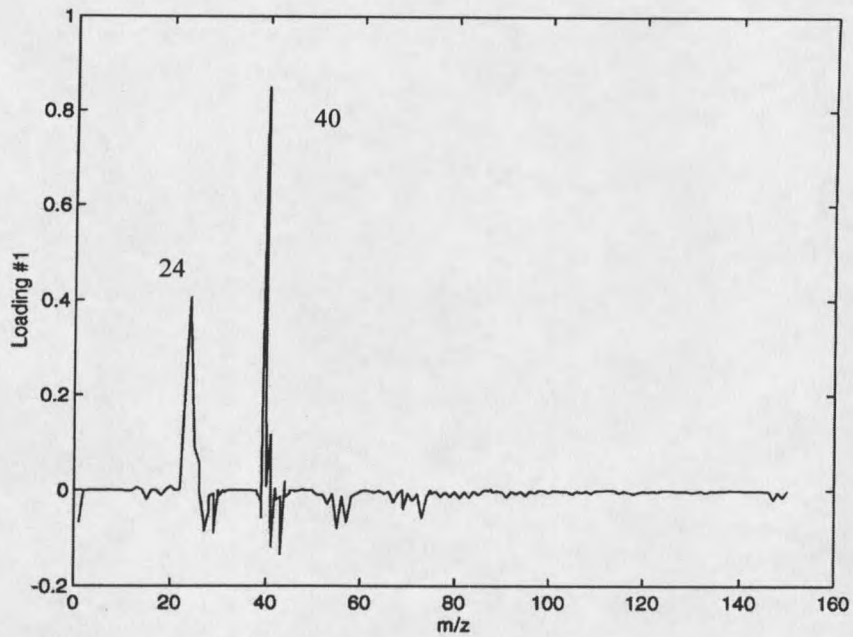


Figure 27. Loading #1 shows a variance in magnesium concentration ( $m/z = 24$ ) and calcium concentration ( $m/z = 40$ ) in the treated fiber group.

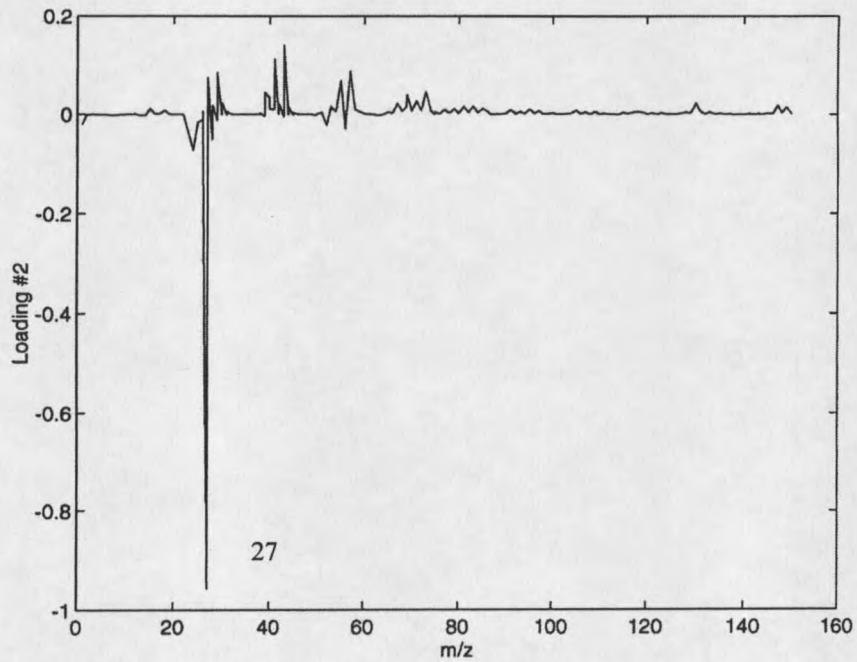


Figure 28. Loading #2 shows a variance in aluminum concentration ( $m/z = 27$ ) in the treated fiber group.

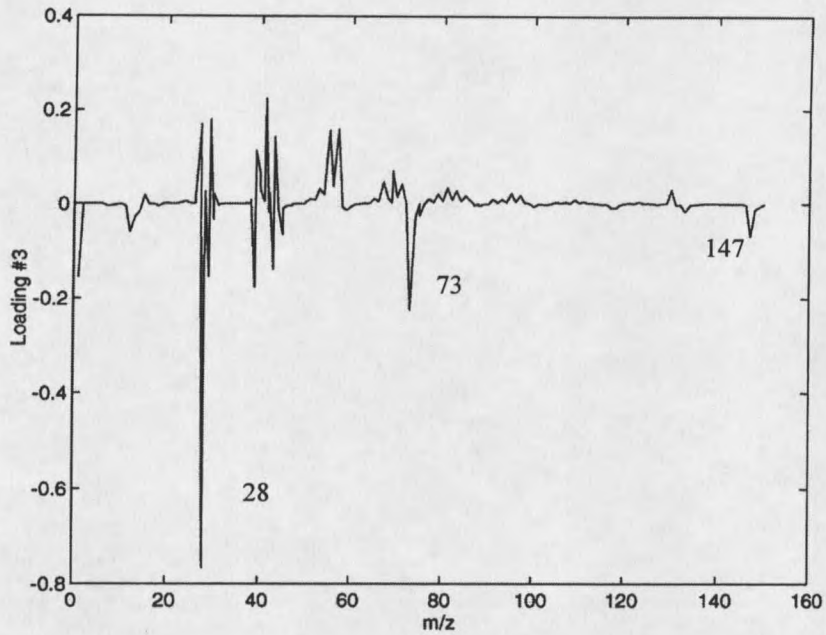


Figure 29. Loading #3 shows a variance in PDMS concentration ( $m/z = 28, 73, 147$ ) in the treated fiber group.

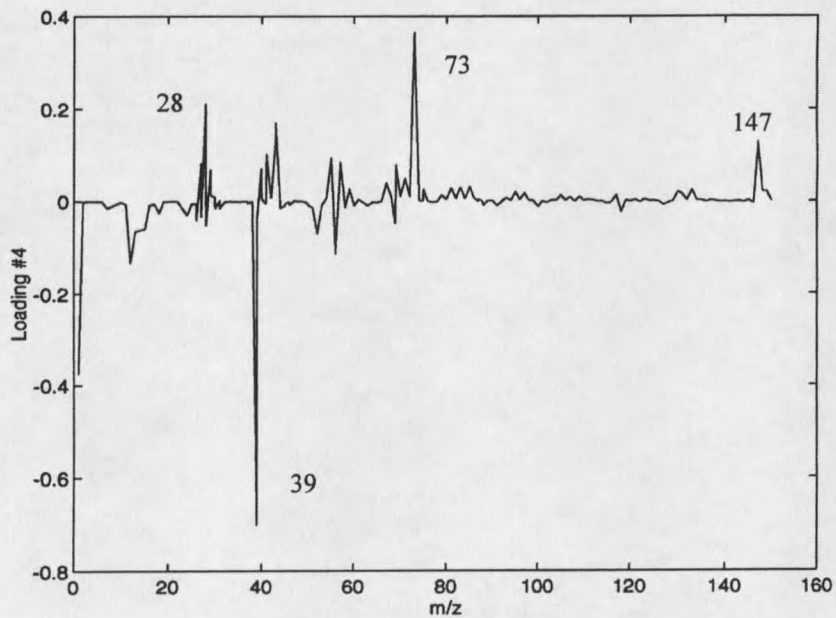


Figure 30. Loading #4 shows a variance in PDMS concentration ( $m/z = 28, 73, 147$ ) and potassium concentration ( $m/z = 39$ ) in the treated fiber group.

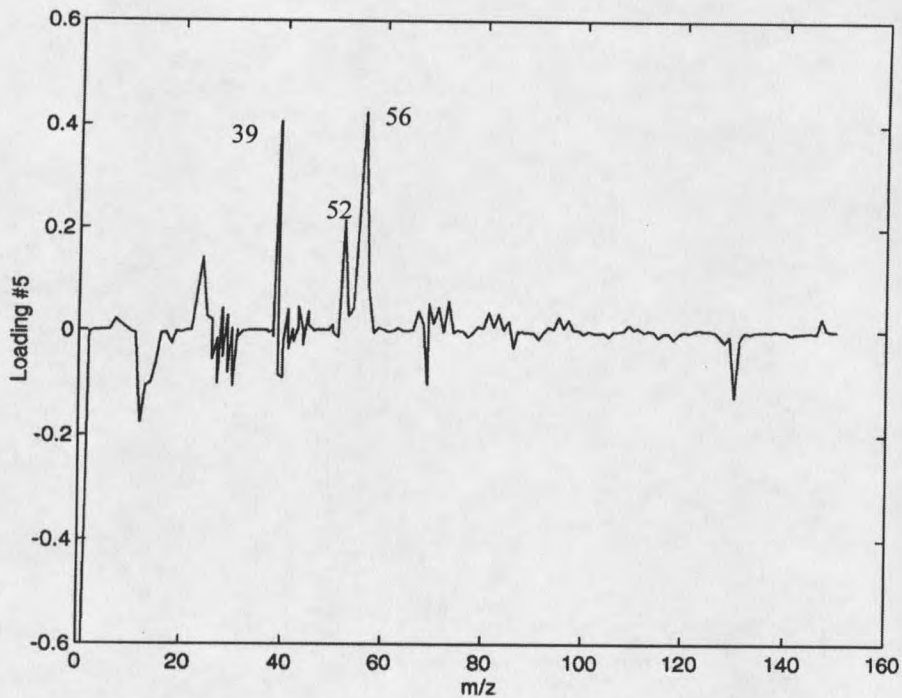


Figure 31. Loading #5 shows a variance in potassium concentration ( $m/z = 39$ ), chromium concentration ( $m/z = 52$ ), and iron concentration ( $m/z = 56$ ) in the treated fiber group.

When looking closer at the individual scores, differences were discovered between good and poor property fibers that differed from what was seen with the untreated fibers. Differences between lots were also noticed. As seen in Figure 32, the good property fibers could be distinguished from the poor property fibers by looking only at principal component number 1, believed to be magnesium and calcium dependent. Although principal component number 5 was not able to separate the poor property fibers (D1234-6A and D1424-6C), it appears to separate the good specimens (D1374-6A and D1390-6A). This would indicate a difference in the amount of potassium, chromium, and iron from one good property lot to another.

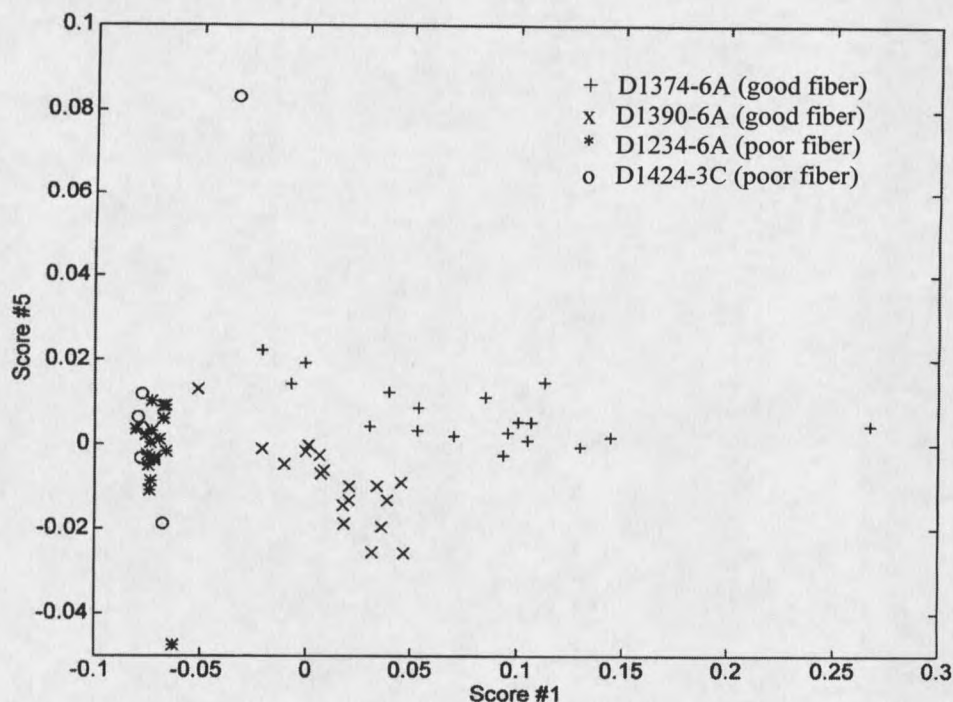


Figure 32. Variations in score #1 (magnesium and calcium intensity) and score #5 (potassium, chromium, and iron intensity) are present in the treated fiber lots.

Discriminant analysis and cross validation was done to confirm the possible differences between good and poor fibers. The weighted mean average did separate the two groups of fibers using 4 principal component scores (Figure 33) with an F value of 35.1 representing a 99.9% confidence level of difference (Table 9). The contributing loadings and m/z values can be seen in Figure 34. Note the magnesium, and calcium positive loading peaks ( $m/z = 24, 40$ ) along with peaks representing potassium, aluminum, and PDMS ( $m/z = 39, 27, 73, 147$ ) and elemental silicon ( $m/z = 28$ ).

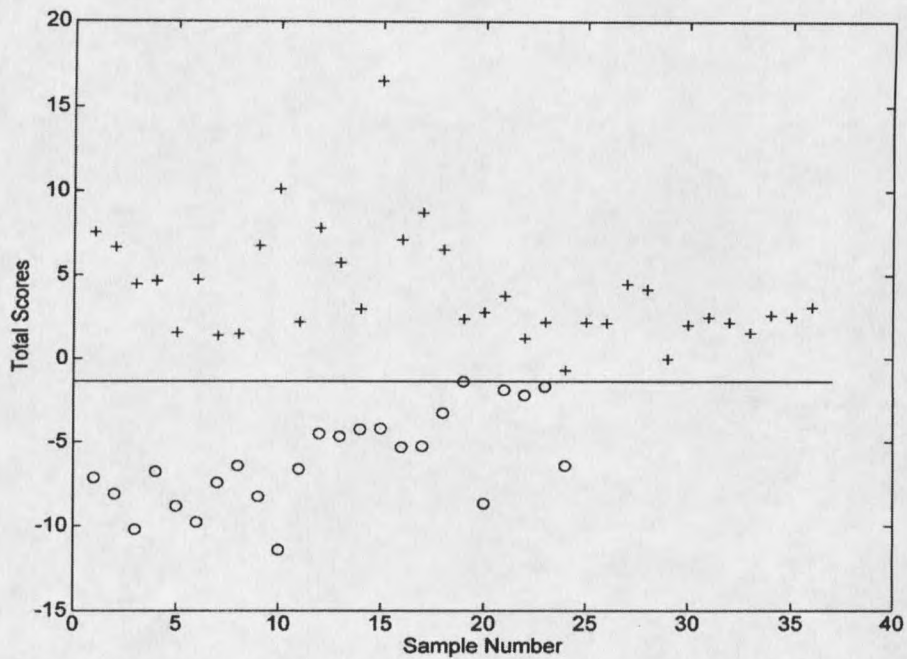


Figure 33. Discriminant analysis with cross validation correctly identified differences between good and poor property treated fibers.

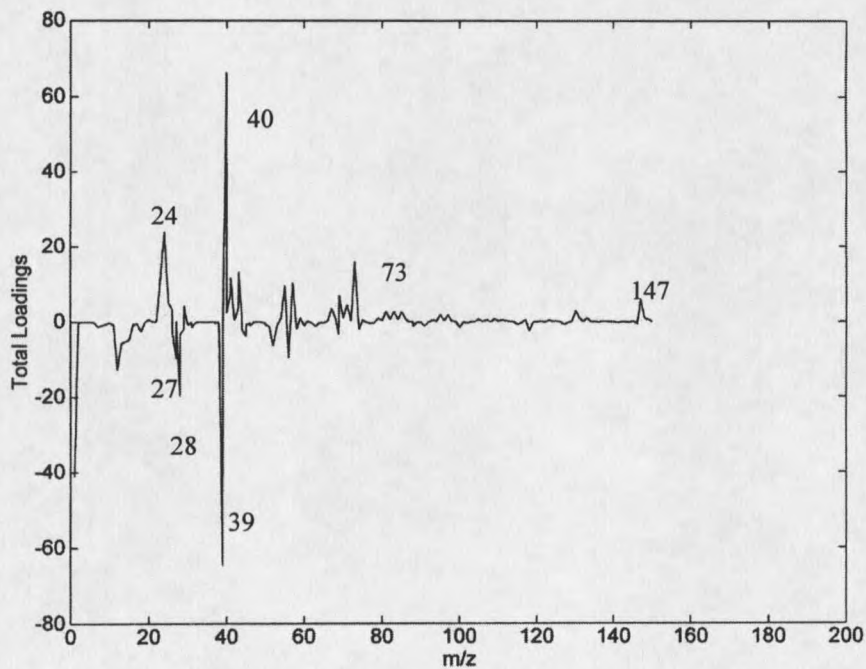


Figure 34. Discriminant loadings show the differences in good and poor treated fibers can be attributed to primarily inorganic elements.

Although the only clearly identifiable loading component using the treated organic peaks was PDMS (Figures 35 and 36), the good and poor fibers could still be separated using discriminant analysis and cross validation. The weighted mean average value separated the specimens using 16 principal components as seen in Figure 37 with an F value of 14.3 and a confidence level of 99.9% (Table 9). The loadings for the cross validation calculations can be seen in Figure 38. Utilizing these discriminant loadings, it can be seen that after the surface treatment procedure, the good property fibers have more unsaturated hydrocarbon characteristics than the poor property fibers while the poor fibers have an increase in the number of nitrogen containing fragments (Appendix E).

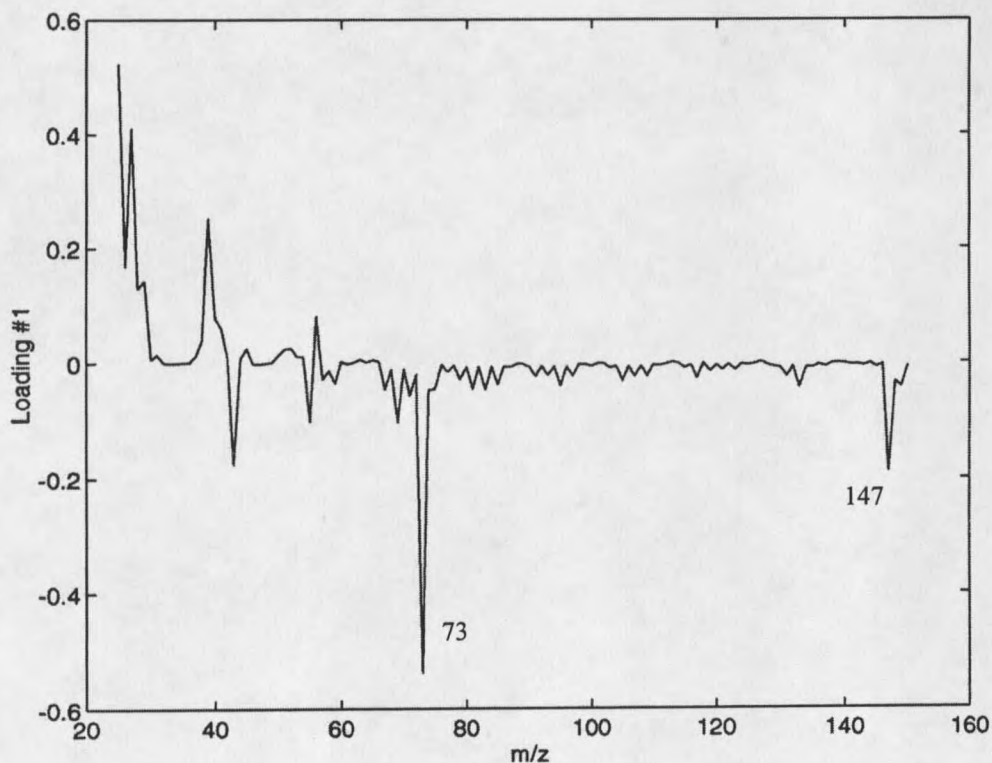


Figure 35. Loading #1 shows a variance in PDMS concentration ( $m/z = 73, 147$ ) in the treated fiber group.

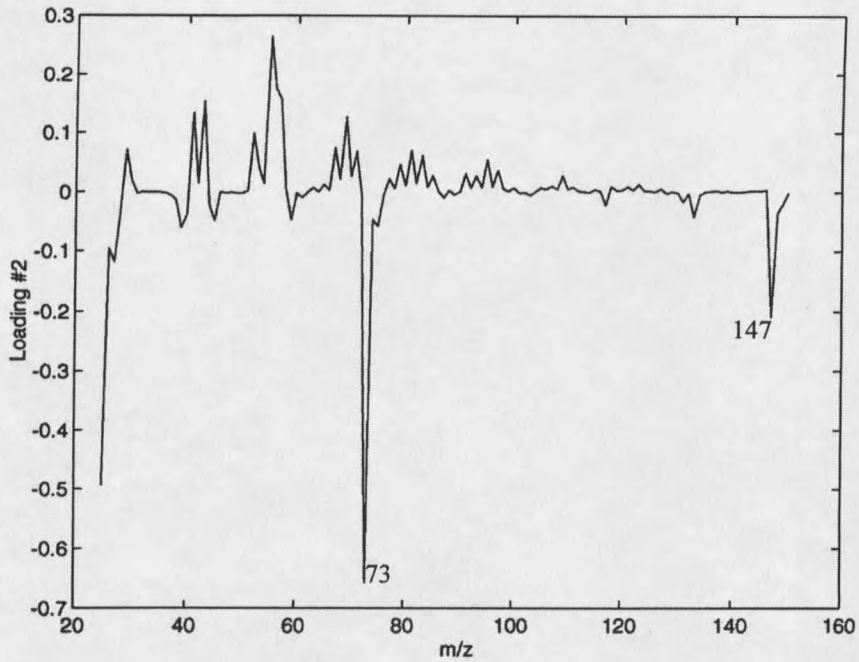


Figure 36. Loading #2 shows a variance in PDMS concentration ( $m/z = 73, 147$ ) in the treated fiber group.

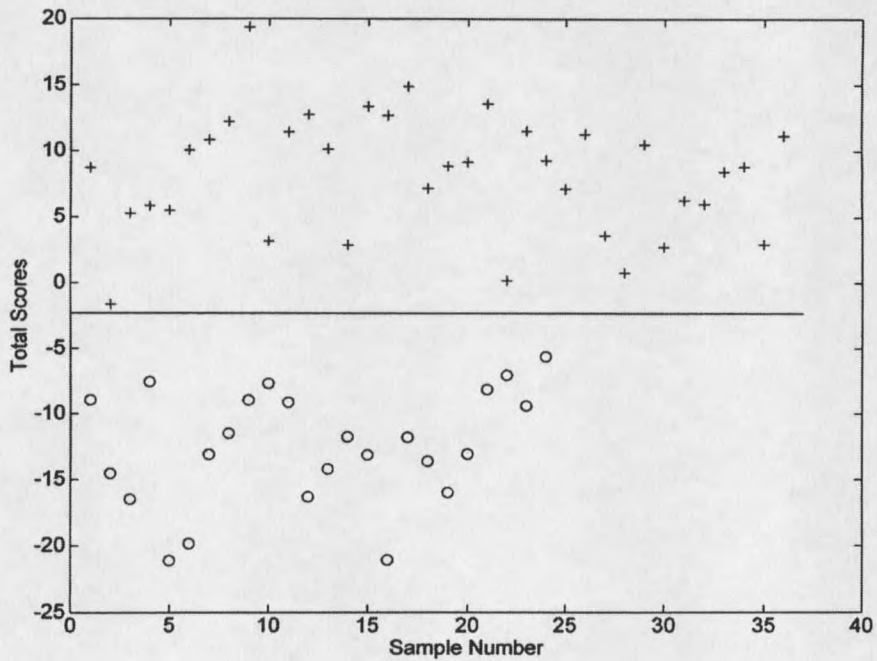


Figure 37. Discriminant analysis with cross validation correctly identified differences between good and poor property treated fibers using organic components.













































































































































































































































































































































































